MASTER THESIS

Design and Development of a Tunnel Magnetoresistance (TMR) magnetometer for LISA

Ankit Kumar Nath

SUPERVISED BY

Dr. Juan Ramos Castro (UPC,IEEC)
Dr. Miquel Nofrarias(ICE CSIC)

Universitat Politècnica de Catalunya
Master in Aerospace Science & Technology
October 2018

This Page Intentionally Left Blank

ABSTRACT

Gravitational waves are a prediction of Einstein's General Relativity recently detected by the on-ground laser interferometers LIGO. LISA (Laser Interferometer Space Antenna) is an ESA mission with expected launch in 2034 aiming to detect gravitational radiation by putting three satellites in heliocentric orbit separated 1 million km one from each other, forming a triangle. The Gravitational Astronomy group at the Institut de Ciències de l'Espai (IEEC-CSIC) has provided the Data and Diagnostics Subsystems of LISA Pathfinder, a precursor mission launched in December 2015 that successfully proved the key technologies to reach the purest free-fall in space to the date, i.e. down to the sub-femto-g [1] .

Our group is currently developing the techniques required for future gravitational wave detectors in space. A particular interesting challenge is the magnetic diagnostic subsystem [2] which requires to reach sensitivities below 10nT/sqrt(Hz) down to the very stable measuring bandwidth of 0.1 mHz. On top of that, the sensors need to be located close to the free-falling test mass ---a condition that can not be achieved with fluxgate sensors.

For that reason, our group already started the development of a magnetic diagnostic subsystem by means of an Anisotropic Magnetoresistors (AMR) [3]. This would allow several improvements when compared to fluxgate sensors: (i) a more compact design, allowing a more of these sensors to be distributed in the spacecraft improving the spatial resolution of the magnetic field mapping; (ii) low magnetic and thermal back-action enabling a closer location to the TM and (iii) low noise performance in the LISA band down to 0.1 mHz.

The current work would be to study an improved design using a new available sensor technology, the so called Tunnel Magnetoresistance (TMR) which would allow and increased sensitivity when compared with the AMRs. This will require the re-design of the signal conditioning circuits for the sensors and the noise and thermal stability characterization of the new design in the frequency range of LISA (0.1 mHz to 0.1 Hz).

ACKNOWLEDGEMENTS

" Scientists have become the bearers of the torch of discovery in our quest for knowledge " - **Stephen Hawking**

Table of Contents

List of Figures

List of tables

Chapter 1

INTRODUCTION

The existence of gravitational waves was predicted by Albert Einstein in 1916 as part of the theory of general relativity[10]. According to Einstein's theory, gravitational waves are ripples in the space-time curvature, which manifests themselves as fluctuating tidal forces on masses in the path of the wave. It was recently detected by the ground based laser interferometer LIGO. LISA (Laser Interferometer Space Antenna) is an ESA mission with an expected launch date in 2034 for detecting gravitational radiation by putting three satellites in heliocentric orbit separated 2.5 million km one from each other, forming a triangle.

The Gravitational Astronomy group at the Institut de Ciències de l'Espai (IEEC-CSIC) has provided the Data and Diagnostics Subsystems of LISA Pathfinder, a precursor mission launched in December 2015 that successfully proved the key technologies to reach the purest free-fall in space to the date, i.e. down to the sub-femto-g [1]. The research group of Gravitational Astronomy is currently developing the techniques required for future gravitational wave detectors in space or rather the next stage of development for the LISA mission. A particular interesting challenge is the magnetic diagnostic subsystem which requires to reach sensitivities below 10nT/sqrt (Hz) down to the very stable measuring bandwidth of 0.1 mHz. On top of that, the sensors need to be located close to the free-falling test mass ---a condition that cannot be achieved with the current fluxgate sensors used in LISA Pathfinder mission.

The goal of this thesis is to develop an improved magnetic diagnostic system based on the technology of magnetic tunnel junction devices which would provide low noise performance characteristics in the low frequency domain.

1.1   Scope and Objective :

The Gravitational Astronomy research group started the development of a magnetic diagnostic subsystem by means of an Anisotropic Magnetoresistors (AMR). This would allow several improvements when compared to fluxgate sensors: (i) a more compact design, allowing a more of these sensors to be distributed in the spacecraft improving the spatial resolution of the magnetic field mapping; (ii) low magnetic and thermal back-action enabling a closer location to the TM and (iii) low noise performance in the LISA band down to 0.1 mHz.

It has already been seen and tested that chip-scale magnetoresistive sensors are a solution to the disadvantages faced while the bulky fluxgate magnetometers were used for LISA Pathfinder. Different noise reduction techniques are being tested such as the flipping technique which has helped to overcome a significant part of 1/f noise, which is always not possible to avoid using the conventional technique of lock-in amplification, only.

Another source of excess noise below 1 mHz is exhibited due to coupling to temperature causing the sensor to be dependent on temperature variations. It has been experimentally seen that using electromagnetic feedback in the signal conditioning circuit has effectively reduced this excess noise [11]

By combining both these methods, the equivalent noise spectral density has been in balance with the noise requirements and by using these noise reduction techniques on AMR, it has been identified as a potential alternative to fluxgate magnetometers for the next LISA mission [3]. The AMR sensor used for carrying out tests were HMC1001 and HMC1002 [12].

The current work would be to study an improved design using a new available sensor technology, the so called Tunnel Magnetoresistance (TMR) which would allow and increased sensitivity when compared with the AMRs. This will require the re-design of the signal conditioning circuits for the sensors and the noise and thermal stability characterization of the new design in the frequency range of LISA (0.1 mHz to 0.1 Hz). The TMR sensor found compatible for our project is TMR9112 [13] which is being used for different experimental purposes and we have had some preliminary results which shows that TMR9112 sensor has a higher sensitivity integrated with a flipping circuit which itself has helped us in reducing the noise significantly, so that it can take measurements in a low frequency range.

This TMR sensor is currently being implemented on a signal conditioning circuit and tested for further verifications to justify our purpose of the experiments. The significant advantages that we have validated about this sensor are :
   • It has a small offset, low hysteresis and a low thermal stability.
   • It is also compatible for high range of voltage supplies.
   • The equivalent noise spectral density is 150 pT/ $\sqrt{}$ Hz at 1 Hz

1.2 Thesis Overview

   This master thesis comprises of six different chapters. The first chapter involves a brief introduction along with the scope and objective of the project.

   Chapter two consists of a fundamental study of gravitational waves supported with equations and illustrations of their principle of operation. It also describes briefly about the different methods of detection , sources and a brief note on the detectors currently present in ground and space for detecting gravitational waves.

   Chapter three starts with an overview of the LISA mission explaining the concept of the mission. It is followed with a description of the LISA Pathfinder mission which is a mission technology demonstrator and a part of the main LISA mission. It has been explained which primitive technologies pertaining to the main LISA mission has been tested already in space, the different subsystems of the LPF mission. This chapter also introduces the magnetic diagnostic unit of the LPF mission for analyzing the contribution of magnetic acceleration noise to the total acceleration noise. There is a magnetic measurement unit which explains the process used to measure the magnetic field with the help of fluxgate magnetometer for the LPF mission.

Chapter four is the core of the masters thesis as it starts by detailing the noise requirements of the improved magnetic diagnostic system. It includes the different types of solid state magnetic sensors, even though it is mainly focused on TMR and AMR sensor and their respective working principle, noise requirements, characteristics and sources of noise. It also explains in brief the other types of magnetic sensors and the different commercial magnetic sensors that are available in the market and to check whether it serves the objective of the mission. This chapter also involves the different

noise reduction techniques used in order to reduce the intrinsic noise of the sensor. This is followed with the front end electronics that involves the schematics of the signal conditioning circuit and equations that governs the functioning of the electronic components that is being used for tests and measurements of the TMR and AMR sensor. It involves the certain changes made in the existing circuit for adapting the circuit to fulfil the requirements of the mission.

Chapter five involves the results obtained from the simulations of the signal conditioning circuit output of the front end electronics , instrument amplifiers and the commercial magnetic sensors that had been used for the purpose of this thesis. It also involves in drawing inference from the results obtained, in order to understand the feasibility of the components used for the different tests that had been made with the front end electronics.

Finally, Chapter six is conclusion which aims at comparing the results obtained and discuss the feasibility of using TMR sensor as a prospective magnetometer for the LISA mission.

It will be followed by the last two sections Bibliography and Appendix.

Chapter 2

Gravitational Waves and Detector

Gravitational Waves can be understood as ripples in the stiff and tough fabric of space-time that propagate at the speed of light, and this phenomena was predicted by Albert Einstein[14], and it is caused by some of the most energetic and violent processes in the universe, with its source originating from compact binary stars, spinning neutron stars, collision or merger of two black holes, neutron star birth and remnants of Gamma Ray bursts [15]. In 1916, it was suggested by Albert Einstein that gravitational waves could be a possible outcome of his General Theory of Relativity, which states that very massive accelerating objects orbiting each other should wrinkle space-time in such a way that these distortions would radiate across the cosmos, like ripples spreading across a pond at the speed of light. Gravitational Waves have two polarization states which will instigate relative directions between free falling bodies to expand in a direction, while contracting in the other direction. The polarizations transverse to the direction of propagation of wave are designated as cross polarization "X" and plus polarization "+". These transverse polarizations produce effects on a ring of free falling test masses that can be seen in the following Figure 1 [16] [10].
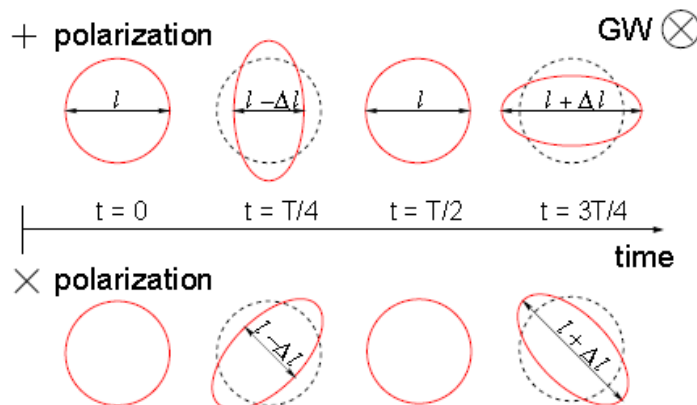
Fig 1: Polarization states of a gravitational wave. Dashed lines indicate the initial position of the bodies. [3]

In order to derive the amplitude of a GW, it is characterised by the strain h of the GW, given by the following equation 1 :

$$h = 2\frac{\Delta l}{l}$$
                                                                                (2.1)

where Δl stands for the relative change in measurement caused due to the GW in the initial arm length l between the masses. Therefore, it would be one of the solution to extend the length of the arm in order to observe changes which are relatively large. However, it is difficult to detect GW, due to the weak interaction of the gravitational radiation with matter. The search for gravitational waves reportedly goes back 50 years ago, with the experiments conducted by Joseph Weber using 'Weber Bars', a kind of

resonant mass detectors. The efforts in detecting gravitational waves was unsuccessful in the beginning, but the initial pioneering effort has already created curiosity among the scientific community which led to the growing interest in gravitational wave detection [17]. Rainer Weiss laid the foundation of the current day gravitational wave interferometers in an early work [18]. Due to the advancement of technology, laser interferometers gained the potential to achieve better sensitivity as it has a much broader band. There were subsequent development in the detector technology, which resulted in the improvement of interferometer arms using Fabry-Perot cavities, which increased the time of exposure of the laser light to the gravitational wave, introducing a "recycling" mirror between the beam-splitter and the laser, in order to effectively increase the laser power and another mirror was introduced between the photodetector and beam splitter which would allow tuning of the interferometer's frequency response [15].
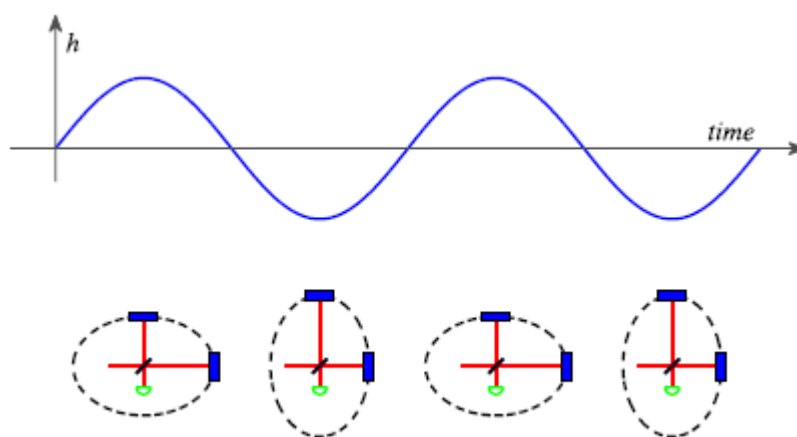
Fig 2 : Carbon illustration of the effect of a gravitational wave on the arms of a Michelson interferometer, while the readout photodiode is denoted by the green semi-circle [4]

The concept of laser interferometer became more developed with the arrival of LIGO , the Laser Interferometer Gravitational Wave Observatory for detecting GW's originating from astrophysical sources. The different astrophysical sources of GW's that LIGO has detected are – five binary black hole mergers and 1 neutron star binary merger. The first detection that occurred in 2016 was the PRL 116, 061102. LIGO works in the principle of Michelson interferometer as shown in Fig 3, as it uses three Michelson interferometer of specialized standards. It is located in Hanford where it houses two interferometers, a 2km long H2 detectors and 4km –long H1. They are capable of sensing GW's in the frequency range 40-7000 Hz and it can even detect a strain amplitude of 10^{-21} Hz [4].There are other GW detectors with long baseline such as Virgo in Italy (a joint Italian / French venture)[19]; GEO600 in Germany (built by a consortium of University of Glasgow, University of Hannover, Max Planck Institute)[20] and TAMA 300 project in Japan [21]. The space borne detector called LISA is a joint NASA/ESA venture as a L class mission within the framework of Cosmic Vision programme of ESA [22]. Currently, an upgrade of technology is going on for Advanced LIGO and Advanced Virgo for discovering newer astrophysical sources of GW's.

Chapter 3

Laser Interferrometer Space Antenna (LISA)

3.1 Mission Overview

LISA is an ESA led mission with contributions from NASA, a space borne observatory to detect GW's in space under the framework of ESA's Cosmic Vision programme as an L3 mission with an aim to study and directly detect low-frequency gravitational radiation between 0.1 mHz and 1 Hz [23]. It is not possible to observe something at this bandwidth from Earth, but it is supposed to reveal some of the most interesting GW sources. This experimental concept of space borne interferometer has simplified many important aspects with respect to ground based interferometers. For example, the micro-gravity environment is generally suited to free floating masses, which eliminates the need for complex seismic isolation systems.

LISA has different scientific goals and among them, the important goal is to track the merger and growth of massive black holes and their host galaxies. The binary black holes comprising of 10^5-10^7 solar masses will coalesce within frequency band of LISA. At large redshifts, LISA will be able to trace these mergers and precisely determine the parameters of the black holes. Another important scientific goal of LISA is to observe the fall of compact objects into supermassive black holes. LISA will perform high precision mapping of the space-time around massive objects in galactic nuclei in order to provide quantitative observational tests of General Relativity. The populations of these stellar mass binaries, will be surveyed, mostly white-dwarf binaries, neutron stars or black holes. The study will provide a detailed analogy about the structure of the galaxy and provide great insight into the dynamics in galactic nuclei [24].

Its current design is quite similar to the generic LISA concept [24] where it will be a constellation of three spacecrafts, forming the vertexes of an equilateral triangle with arm lengths of LISA being approximately 2.5 million kilometres. This observatory has been moved to space in order to facilitate the arms to be made very long, which in turn will relax the displacement sensitivity by six orders of magnitude with respect to ground based interferometers and due to the quietness in space in terms of thermal, magnetic and seismological environment and it eliminates the major disturbances to the test masses, which generally limits the ground based detectors at low frequencies. This helps us to explore the region of the gravitational wave spectrum below 1 Hz. The constellation of LISA is in a heliocentric, earth trailing orbit with an approximation of 20 degrees behind Earth. At an inclination angle of 60 degrees, the constellation of LISA

is cartwheeling around the sun. This arrangement of orbits produces a constant solar illumination which creates a thermal environment.
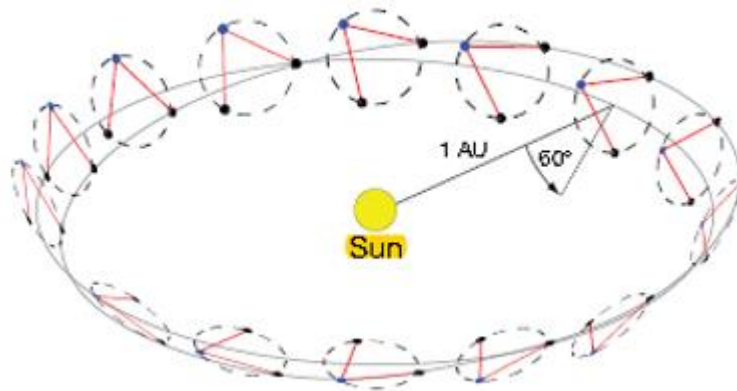
Fig. 3 : Illustration of LISA orbit exhibiting 60º angle of inclination of the LISA constellation plane. The LISA constellation trails the Earth by an angle of 20º [25]

However, fewer things are complicated in space such as the arm lengths will change by tens of thousands of kilometres over a year, owing to the perturbations caused by the Earth's gravity or problems that arises due to poor launch mechanisms and inappropriate orbit design. The arm lengths of the spacecraft cannot be fixed since there is no way to anchor. These fluctuations in arm length will cause several technical problems. The main aim of LISA is to measure differential accelerations between these pair of test masses , which is translated as gravitational waves , by the use of laser interferometry [2].

3.2   LISA Pathfinder : Mission Technology Demonstrator

The technologies responsible for the LISA mission are highly sophisticated and since it is not possible to fully test some of the hardware on ground, a mission technology demonstrator satellite was developed called LISA Pathfinder, in order to pave the way for the LISA mission. The main objective is of LISA Pathfinder is to reproduce the behaviour of one of the arms of the LISA in a single spacecraft, in order to shrink the optical link between test masses from 2.5 M km to around 37.6 cm. However, such a reduction in the arm length would prevent LPF in the detection of the gravitational wave, and limit it to the technological test bench of the different subsystems to be used by LISA. The sensitivity and frequency requirements of the measurements of LPF is somewhat reduced as compared to LISA. The bandwidth for measurement in case of LPF was restricted from 1 mHz upto 30 mHz and the requirement for differential acceleration noise was set to 3 x 10^{-15} m/s² /√Hz. It means that the requirements for both parameters have been relaxed by one order of magnitude compared to LISA.
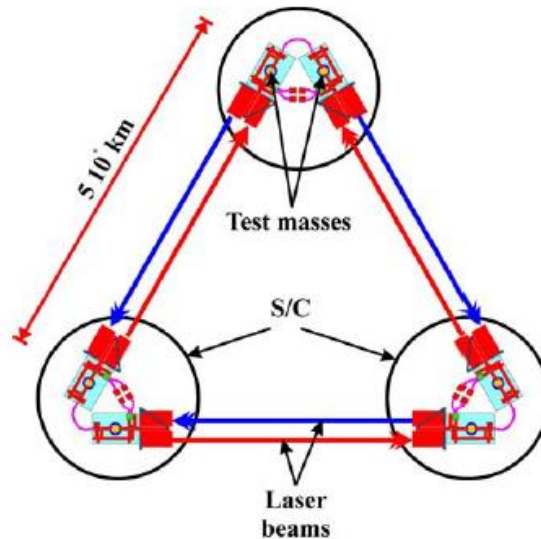
Fig 4 : LISA layout [5]

LISA Pathfinder comprises of two scientific modules : the LISA Technology Package (LTP) [26] , which is the science module provided by ESA and the Disturbance Reduction System (DRS), the scientific module contributed by NASA. The major technologies involved in the LISA Pathfinder mission are the Optical Metrology Subsystem (OMS) and the drag free concept. The drag-free concept comprises of a Gravitational Reference Sensor (GRS), which utilises a set of electrodes to determine the position of the test masses compared to the spacecraft to nanometer precision using capacitance measurements. It returns a signal to the set of micro-thrusters in order to ignite it and relocate the spacecraft so that the test mass remains in the center, thereby preserving the free fall motion of the latter. The OMS provides a precise picometer level measurements of the relative acceleration/position of the two test masses, using precise interferometry.

3.2.1 LTP and Subsystems

LISA Technology Package or LTP comprises of two free floating masses which are made up of an alloy of Au (73%) and Pt (27%), with a mass of 1.96 kg and a distance of 376 mm separating the test masses. The whole experiments and components are hosted within the single spacecraft. A laser interferometer is used to measure the relative motion along the common X-sensitive axis. The test masses are surrounded by the respective position sensing electrodes, hence, these electrodes provide information about the positioning of the test masses relative to the housing frames. The control system of the spacecraft receives information of the sensing electrodes and the laser system, and translates the information into commands for the positioning of the test masses and the spacecraft. The micro-Newton thrusters are commanded by the drag-free control system to keep the spacecraft centred with respect to the position of the test mass 1. The electrode actuation system is commanded by the low frequency control system in order to maintain the coordination of test masses 1 and 2.
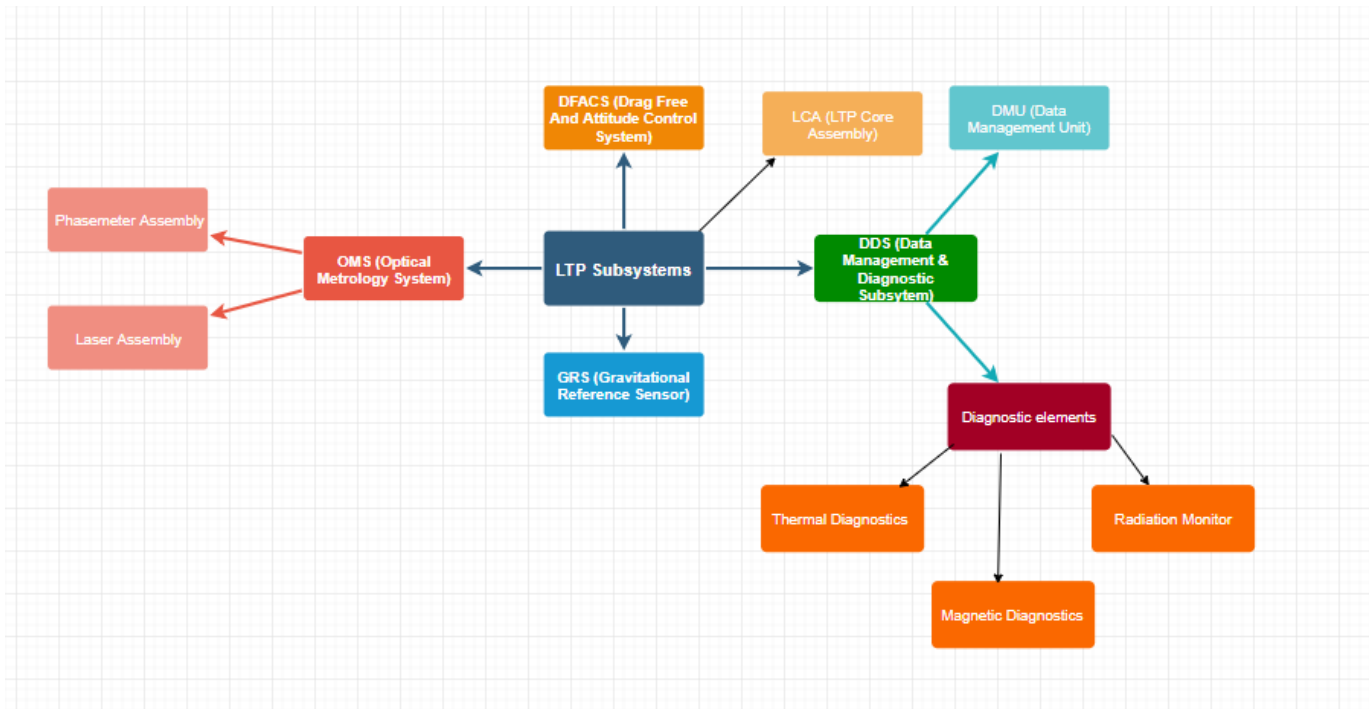
Fig. 5 : Block Diagram of the different subsystems of the LTP

LTP possesses different subsystems for accomplishing these tasks and they are :

1) Gravitational Reference Sensor (GRS) : The GRS subsystem is also known as Inertial sensor (IS). It comprises of a 46 mm-side gold-platinum cube and helps to monitors the motion in all 6 degrees of freedom between the test mass and the spacecraft as well as providing a mechanism, to both release the test masses into free-fall, and when desired mechanically re-grab the TM in orbit. There are two GRS's , one for each test mass. The GRS provides a launch lock or caging device to protect and hold the TM during the vibrations occurring at the time of launch. Another key capability of the GRS's is to discharge the TM from charged particles due to Solar Energetic Particles (SEP) charging and Galactic Cosmic Rays (GCR), periodically and/ or continuously with the help of Charge Management System (CMS). All the subsystems of the GRS are enclosed in a vacuum enclosure.

2) Optical Metrology System (OMS) : The relative displacement between both test masses along the x-axis, is measured by OMS. It will measure the position of TM 1 at the same time as TM 2 ,with respect to the spacecraft.. The total setup of the interferometric system, is based on an optical bench, placed between the two GRS. It comprises of all the fundamental elements, necessary to perform the interferometry. They are :
   - Laser Assembly : It houses the laser source and the unit responsible for modulation.
   - Phasemeter Assembly : It comprises the processing unit and the set of photodiodes.

The data acquired by the phasemeter from the scientific readouts is processed by the Data Management Unit (DMU) .

3) Drag Free and Attitude Control System (DFACS) : In LPF, the drag free environment is created by the action of the control system on the spacecraft. It is known as the DFACS unit and the controller was designed by Astrium GmbH. The controllers allow the selection of different science/controlling modes since it has been modelled with a combination of sensors and actuation selection matrices. The main control mode responsible for scientific purpose is Science Mode 1 which is differentiated into two control loops – low frequency suspension loop and the drag-free loop. Drag free loop acquires the position of the TM 1, w.r.t the spacecraft and transfers the actuation signals to the 12 micro-Newton FEEP thrusters for centering the spacecraft wrt the TM1. While, the differential displacement between TM1 and TM2, is taken as a reference signal by the low frequency suspension loop and it acts on TM2, forcing it to follow TM 1. The algorithms necessary for computation are stored in the On-Board Computer of the spacecraft.

4) LTP Core Assembly (LCA) : The LTP core assembly is placed at the central part of the spacecraft. It is comprised of two parts : Gravitational Reference Sensors and the optical bench between them. The LCA is fixed to the cylindrical wall of a satellite, which is located at a centred position, by the help of 8 struts, in the spacecraft .

5) Data management and diagnostics subsystem (DDS) : The DDS has the most important function, of differentiating among the various noise sources which directly affects the main scientific measurement of the mission, i.e., the phase readout of the interferometer. The DDS plays a crucial role in estimating the effects of each independent disturbance on the parasitic acceleration noise, obtained by certain flight experiments. DDS is comprised of two main parts : data management unit (DMU) and the diagnostics elements. DMU is the computer of the LTP and it's tasks involve : controlling and driving the diagnostics system ; acquiring and processing of the phasemeter data. The diagnostics elements of the DDS is comprised of a number of sensors (magnetometer, thermistors and a particle detector) and actuators (coils and heaters). The researchers from the Spanish LTP group, which is comprised of teachers, researchers and students from UPC, ICE/CSIC, IEEC and IFAE were responsible of the design and development of this subsystem. The work being presented in this thesis , is devoted to the design and development of an advanced space magnetometer of higher sensitivity and low noise so as to detect low frequency GWs.

The DDS comprises of different sensors and actuators which are known as diagnostic elements. The diagnostic elements is referred to the three different type of diagnostics – Thermal diagnostics, Radiation monitor and Magnetic diagnostics. They are the following :

- Thermal Diagnostics : The LTP comprises 14 calibration heaters and an array of 24 high precision thermistors, which are placed at different points within the LCA, such as inertial sensors, the optical bench and suspension struts. The thermal environment is monitored by the sensors along the measurement bandwidth at a sensitivity of 10^{-5} K/√Hz. The measurements on temperature is

translated as test mass acceleration noise. High signal to noise ratio thermal signals are applied by means of calibration heaters (active part), which helps in establishing the relationship between temperature measurements and acceleration noise of the test mass.

- Radiation Monitor : The LPF was hit by several charged particles when it was placed in the Lissajous orbit around the Lagrange point L1 and some of them might reach the TM and cause charge depositions in them. The flux of these charged particles are sampled by the particle detector. The charge deposition is a random process which causes acceleration noise due to the interaction of charged particles with the electric system which controls the position of the test mass. This results in fluctuations of the position of the TMs with respect to the centre. The charge accumulated in the test masses are purged by the help of UV lamps, placed in the LTP. Measurements taken over a longer duration by the inertial sensor would help in establishing average charging rates, but the flux of galactic cosmic rays (GCR) and solar energetic particle events fluctuate temporally which will contaminate the scientific data. In order to establish this correlation between the incident radiation and the TM charging, a radiation monitor is used. This TM charging noise can be minimized by post-processing of the radiation monitor data , or, matching of the charging and discharging rates.

- Magnetic Diagnostics : This system comprises four tri-axial magnetometers and two induction coils , in the case of LISA Pathfinder. But, in LISA , the magnetometers that are proposed to be used are AMR and TMR. The magnetometers senses the evolution of magnetic field with high precision while the coils placed beside the test masses and the GRS towers, generates magnetic field in a controlled manner within the volume of the test masses to eventually produce calibration inputs. The fluctuations in the acceleration are caused due to magnetic field gradient, residual magnetic properties of the TM and the magnetic field in the region of the test mass. In order to determine the transfer function relating the magnetic forces and the effect on the motion of the TMs , we use magnetometers and induction coils.

The purpose of LISA Pathfinder was not to detect gravitational waves. The mission was intended to validate the technologies and overcome technical challenges, in order to foresee that the full-scale mission of Laser Interferometer Space Antenna (LISA) is possible. The full scale mission will have three 2.5-million-kilometer long arms while in LISA Pathfinder , one of the arms shrinks down to 38 centimeters (15 inches) which is placed in a single spacecraft. LPF was designed to measure relative motions of the two test masses on the picometer scale, around a trillionth of a meter. The final results that was received from LPF exceeded the limit and the measurements reached to femtometer scale, atleast five times better result than it has been expected. The noise resulting from the collisions between the test masses and the stray molecules was seen to die down, as the vacuum chamber vented out the gas particles to space. The two test masses has been found to be almost motionless with respect to one another, with a relative acceleration which is lower than ten of millionths of a billionth of Earth's gravitational acceleration, g.
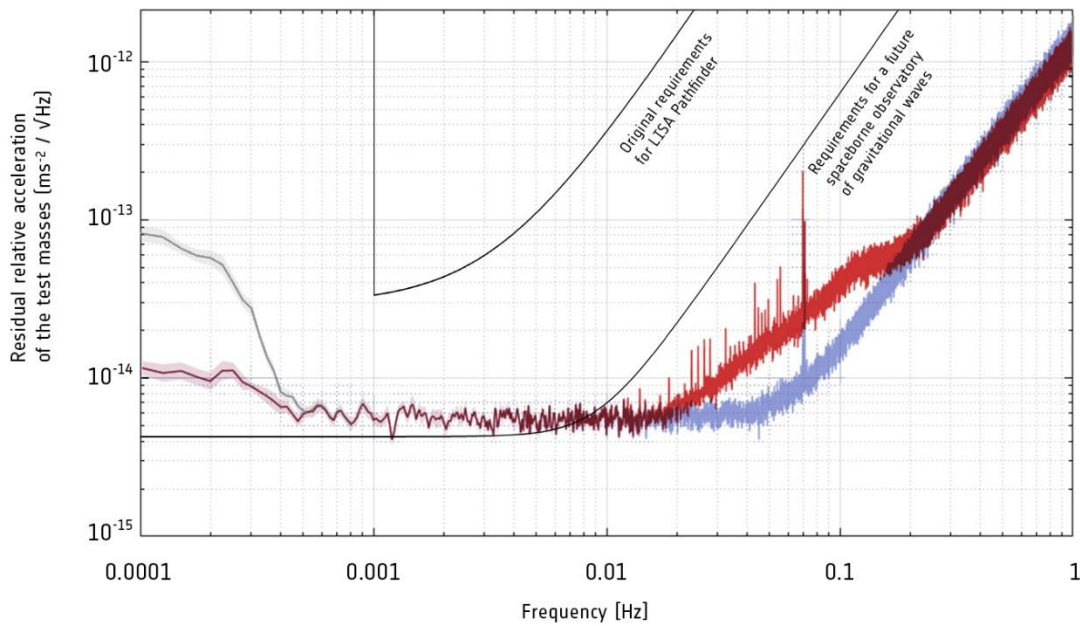
Fig. 6 : This graph depicts the residual relative acceleration of the two test masses on LPF mission as a function of frequency [6]

The team of researchers who had been working on LISA Pathfinder were able to measure the remaining forces acting on the test masses, and found out that there are three major sources of noise, depending on the frequency. The scientists have found out from the result that there is a small centrifugal force acting on the TMs , which is caused due to the rotation of the space-craft, which can be partially corrected thanks to the star-tracker read-out. The precision of the LPF is limited at higher frequencies, between 60 mHz and 1 Hz , by the sensing system of the OMS which is being used to monitor the orientation and position of the TMs. While, at lower frequencies between the frequency range, 1-10 mHz, the performance is limited by gas particles bouncing on the test mass surfaces. However, this limitation starts to reduce as more molecules starts venting out to vacuum in space. Nonetheless, the performance of LPF systems has surpassed the level of precision required for the future LISA mission by a factor of 100. Thus the technology demonstrator mission , LPF, has precisely validated some of the key technologies to be used in LISA for the detection of gravitational waves originating from extra galactic events in space.

3.3 Magnetic Diagnostics System of LISA

This chapter elaborates the detailed characteristics of the magnetic diagnostics subsystem for the LISA Pathfinder Technology Package (LTP) which is quite alike LISA mission. The magnetic diagnostic system of LTP is the hardware subsystem that is supposed to deliver the measurements necessary for estimating the contribution of magnetic acceleration noise to the total acceleration noise. The main goals of this diagnostic system are :creation of controlled magnetic field and gradients, and the measurement of DC magnetic field values and the fluctuations that it sustains, within the bandwidth of its measurements at varied locations of the LCA [27]. The magnetic diagnostics system comprises two main subsystems – the on-board magnetic coils for

magnetic field generation and magnetic measurement unit. The hardware has been validated by different tests to fulfil the mission requirements and the instrumentation associated with these tests have been discussed in this chapter. The main drawbacks that was faced while developing the subsystem has also been highlighted.

3.4 Magnetic measurement unit

  The size, weight, and the power restrictions are strictly applied while designing the on-board instrumentation for LPF, however, one of the main constraints faced while designing is the long term stability, that limits the noise performances at low frequencies. Therefore, the DC magnetic requirement and the fluctuations at the location of the TM displayed in the table 2.1, are needed to be fulfilled by the magnetic measurement unit [3].
  The noise level of the magnetic sensors and the associated readout electronics are limited by the magnetic fluctuations that is estimated for the spacecraft. It requires the noise level of the magnetic measurement unit to be at least an order of magnitude less than the value   of the maximum estimated magnetic fluctuations. Therefore the magnetic measurement unit has to comply with a noise figure of :

$$S_{B,system}^{1/2} \leq 10 \ nTHz^{-\frac{1}{2}}, 1mHz \ \leq \frac{\omega}{2\pi} \leq 30mHz \qquad (3.1)$$

The milli-hertz range of the measurement bandwidth for the noise performance has been hardly explored and only on certain occasions, the specifications are mentioned by the manufacturers of the electronics components. This unit has other different requirements other than the ones which has been already mentioned before, such as, the unit is required to have a field measurement range of ± 60 µT and the end of the scale has a better uncertainty than 1%.

Table 3.1 : DC requirements and fluctuations estimated in the TM locations for LISA Pathfinder

DC requirement	ASD estimation
$\lvert B_{bg} \rvert \leq 10\mu T$	$S_B^{\frac{1}{2}}(\omega) \leq 100 \ nTHz^{-\frac{1}{2}}$
$\lvert \nabla B_{bg,x} \rvert \leq 5\sqrt{3}\mu Tm^{-1}$	$S_{\nabla Bx}^{\frac{1}{2}}(\omega) \leq 250\sqrt{3} \ nTm^{-1}Hz^{-\frac{1}{2}}$

3.4.1 Description of the Magnetometer for LPF

The measurement of the magnetic field and gradient fluctuations at the location of the test masses is not possible. The estimation regarding such measurements are made at varied selected locations. It has been concluded from previous studies [28] which has led to the placement of only 4 magnetometers within the volume of LCA. The specific positions of measurements has been listed in the table 2.2. The magnetometers that were selected for LISA mission were space qualified fluxgate magnetometers. This technology was chosen because of its low noise, high sensitivity

and since it has been used previously in different space missions, fluxgate devices were considered as the most preferred solution.

The space grade magnetometer selected for this mission is an ultra-miniature triaxial fluxgate device (TFM100G4) which has been designed by Billingsley [9] and it is high reliable. These magnetometer by construction comprises of three different magnetic sensors, along the x-, y- and z- directions. The fluxgate magnetometer consists of a secondary coil, for each of the axes along the x-, y- and z- axes, which surrounds the inner primary coil around the magnetic core, that is made up of high permeability material [27].
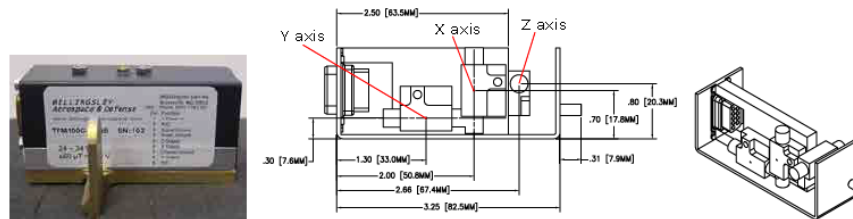
Fig 7 : Left : Engineering model of the Billingsley triaxial fluxgate magnetometer selected for LISA Pathfinder. Center and Right : mechanical drawing of the inner sensor heads (X, Y and Z axis) [3]

Fig. 8 : The four tri-axial fluxgate magnetometers in the payload of LISA Pathfinder. The TMs (solid gold cube) are located at the centre of each electrode housings (cubic structures) placed inside the vacuum enclosure (cylinders) [3]

Despite being a small sensor within the family of low noise fluxgate devices, this magnetometer is bulky(94 cm³) , comprising of long ferromagnetic heads (~2cm long), and each triaxial magnetometer consumes power equivalent to 0.8 W. These constraints led the placement of only four triaxial sensors at large distances from the TMs (≥18.85cm) to avoid disturbances due to magnetic back-action. The positions of the magnetometer in the LTP is given in the following table 3.2.

Table 3.2 : The position of the TMs and the magnetometers in the spacecraft and their coordinate system is fixed with respect to the spacecraft. The TM centers are connected at the x-axis and y-axis directs towards the solar array along the vertical axis. (Units are in meters) [3].

Item	Order Number	x	y	z
	1	-0.0758	0.3694	0.532
	2	0.0758	-0.3694	0.532
	3	-0.3765	0	0.532
	4	0.3765	0	0.532
Test mass	1	-0.1880	0	0.532
	2	0.1880	0	0.532

The main characteristics of the fluxgate magnetometer within the terms of LPF mission are :
- Repeating long term measurements especially in places where thermal dependences are crucial.
- To distinguish on the basis of noise and resolution.
- Estimation of the accuracy of the measured value along with the linearity and offset values.

The specifications pertaining to the magnetic measurement subsystem of LPF are laid out in the following table 3.3.

Table 3.3 : Specifications of the sensor model Billingsley TFM100G4 ,i.e, magnetic measurement subsystem [9] .

Parameter	Value
Field Range (B_{range})	$\pm 60 \mu T$
Temperature Coefficient (TC)	1.2 nT/K (0.002% FS/K)
Noise Density ($S_B^{1/2}$)	<100pT/√Hz @ 1 Hz
Input Current (I_{supply})	< 60 mA
Input Voltage (V_{supply})	24 – 34 V
Linearity (LSF)	0.015 %
Sensitivity	166.7 $\mu V/nT$
Offset Voltage	< 25 mV (150 nT)
Bandwidth	3.5 kHz
Operating Temperature	-55ºC to +85ºC
Susceptibility to perming	$\pm 20nT$ shift with 0.5mT
Axial alignment	< 1º
Weight	101 g

Chapter 4

IMPROVED DESIGN OF MAGNETIC MEASUREMENT SUBSYSTEM FOR LISA

4.1   Noise requirement of the Magnetic Diagnostic System

The significant characteristics pertaining to the magnetic measurement system has been already discussed before in a previous section. The noise performance at the lower end of the LISA bandwidth (1-10 mHz) is affected by magnetic field fluctuations, spread across the TM, that are being expected to be dominated by a time-varying interplanetary magnetic field not less than 100nT/√Hz [29][30], while it is presumed that the main contributors to the fluctuations of magnetic field gradient are the magnetic sources of the spacecraft [30]. Although, the requirements for LISA at subsystem level and the distribution of the magnetic sources in the spacecraft is still not formally defined, however to be on the safer side, the noise performance of the magnetic measurement unit should be atleast one order of magnitude less noisy than the presumed value of the interplanetary magnetic noise that is going to be measured. To make such a thing possible, the sensitivity of the measurement system is expected to be :

$$S_{B,system}^{1/2} \leq 10 \ nTHz^{-\frac{1}{2}}, \ \frac{\omega}{2\pi} = 0.1 \ mHz \qquad (4.1)$$

The reason for validating the use of TMR sensors as an alternative to the LISA mission scheme with AMR and fluxgate magnetometers, is the size, mass, sensitivity and power restrictions for applications in space. The TMR-type TMR9112 sensor presents the lowest noise level among other different magnetoresistive sensors. However, an important disadvantage of the TMR and AMR sensors is the intrinsic 1/f noise which can be avoided to a great extent with the integrated flipping circuit to reduce the intrinsic noise level (applicable inly for AMR sensor). Hence, it can be used for low frequency applications. Different experimental research that has been conducted in the laboratory in the frequency range between 0.1 Hz and 10 KHz [2], [31], [32] . According to our knowledge, the performance of sensor noise and the associated electronics have not been widely explored at the lower end of the LISA bandwidth (0.1 mHz). In this chapter, we are going to study in details about the low frequency noise characteristics of a prototype board which is based on magnetoresistive sensors with different techniques of reducing noise, necessary for achieving the magnetic noise level for LISA.

4.2   Solid State Magnetic Sensors

4.2.1 Tunnel Magnetoresistive Sensor (TMR)

The TMR sensors are advanced magnetic sensors which utilises a TMR or Magnetic Tunnel Junction (MTJ) element, that is highly-sensitive reproducing element of an Hard Disk Drive (HDD) head. The fundamental theory of the MTJ element is based on the principle of spintronics that makes use of the quantum spin conditions alongwith the electric property of the electron, which is based on the pre-existing theory of electronics. Spintronics drew immediate attention from the international scientific community, when Pr. P. Grunberg and Pr. A. Fert received the Nobel Prize in Physics in 2007 [33].
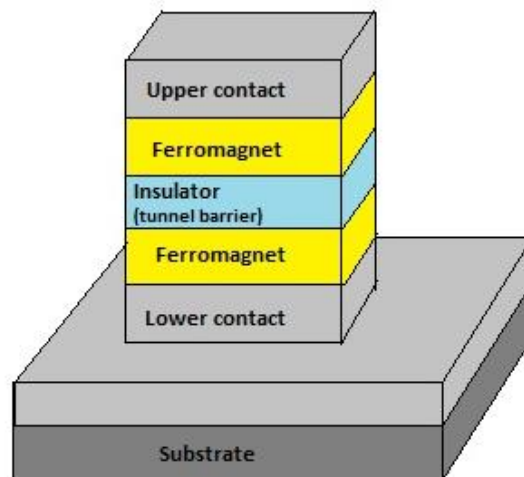
Fig 9 : Schematic of a Magnetic Tunnel Junction sensor

The TMR element has a similar structure as a GMR element and it comprises magnesium oxide (MgO) or aluminium oxide (Al2O3) in between two stacked ferromagnetic layers (free layer/pin layer) made using advanced thin-film element processing technology and it can be seen in the Fig. 3 [7]. However, in the TMR element , the flow of current is perpendicular to the surface of the film while the flow is in the horizontal direction with respect to the film surface in a GMR element. In the TMR element, the electrons in the ferromagnetic layer pass through the insulator by the principle of quantum-mechanical effect and following the tunnelling effect, the electrons are injected in the other ferromagnetic layer [34]. The influence of the external magnetic field in a certain direction changes the magnetization direction of the free layer even though the magnetization direction of the pin layer is fixed. The change in magnetization direction in this free layer changes the electrical resistance of the TMR element. When the directions of magnetization of the free layer and the pin layer are parallel, the electrical resistance becomes the smallest, which causes a lot of

current to flow into the barrier layer. When the directions of magnetization are antiparallel, the resistance is extremely large , and it limits the current flow in the barrier layer. Therefore, the resistance changes depending on the relative angle of the direction of magnetization of the two layers. This phenomenon is known as Tunnel Magneto Resistance (TMR) effect.
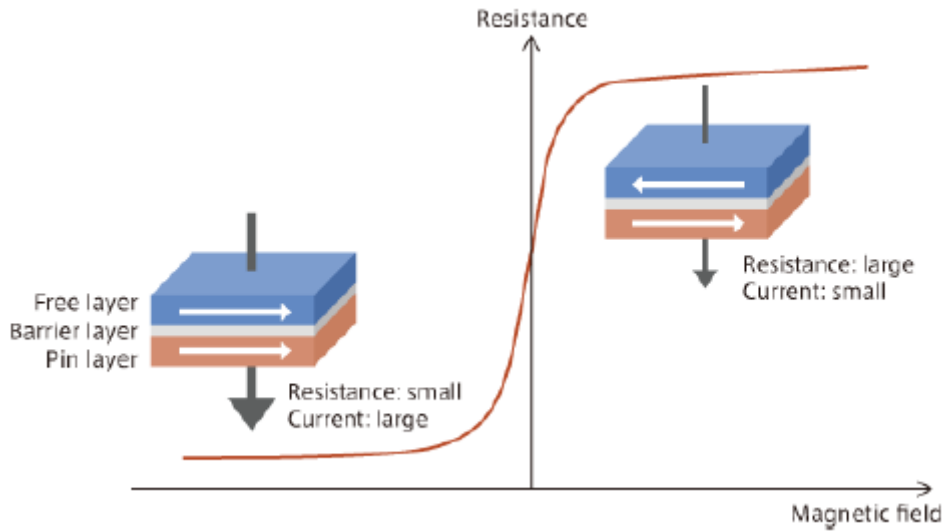
Fig 10 : Representation of a TMR element in a parallel magnetization configuration (Left) and in anti-parallel magnetization configuration (right). The arrow in black represents the current going through the junction. [7]

The resistance of this tunnel junction is given by the formula :

$$R(\theta) = R_o - \Delta R \cos(\theta) \tag{4.2}$$

Where θ is the angle between the sensing layer and the magnetization directions of reference while R_o is the area resistance RA divided by the area of the tunnel junction. The thickness d of the barrier increases with the RA by an exponential function.

$$R \sim e^{d/do} \tag{4.3}$$

The relation above shows that the resistance of the TMR sensor is highly sensitive to the thickness of the barrier. The TMR effect can be described by :

$$\text{TMR} = \frac{R^{max} - R^{min}}{R^{min}} \cdot 100\% \tag{4.4}$$

Where R^{max} is referred to the resistance occurring in the antiparallel orientation of the direction of magnetization (θ = 180 degrees) and R^{min} is the resistance in the parallel configuration (θ = 0 degree). The TMR effects achieved for junctions deposited in industrial production tools can be as large as 200%.

The discovery of the TMR effect at low temperature occurred in 1975 [35]. Although, this discovery did not grab attention at that time since the application was difficult. The

TMR effect came in the spotlight in 1995, when a change of almost 20% of the magnetic resistance was achieved at the room temperature in low magnetic field [36]. The rate at which the resistance changes in the TMR element is expressed by a value called the MR ratio. In conventional AMR and GMR elements, the MR ratios are about 3% and 12% respectively. However, the MR ratio of a TMR element is 100%. The non-magnetic metal (Cu,etc.) in a GMR element, is sandwiched between two ferromagnetic layers, and the electron transfer occurs as electric conduction in the metal. In TMR element, the electron transfer occurs as quantum mechanical tunnel effect. This is the reason, when the directions of magnetization of the free layer and the pin layer are antiparallel, a TMR element exhibits extreme characteristics in which the electrons are not able to move at all, with respect to the characteristics of a GMR in which the conditions are hard for the movement of electrons. It causes a TMR element to portray an extremely large MR ratio. In addition to the large MR ratio, the output characteristics are really distinct, such as "1" or "0" or "Yes" or "No" [7].

This is the reason to use highly sensitive TMR elements as magnetic sensors with a large output characteristics. The following Fig.4 is a comparative analysis of the characteristics of magnetic sensors using a GMR element, AMR element and TMR element (on the application of 5V).

	AMR	GMR	TMR
MR ratio [%]	3	12	100
Output [mV]	150	560	3300
Temperature dependency [%/°C]	-0.29	-0.23	-0.13

(Applied voltage: 5V)
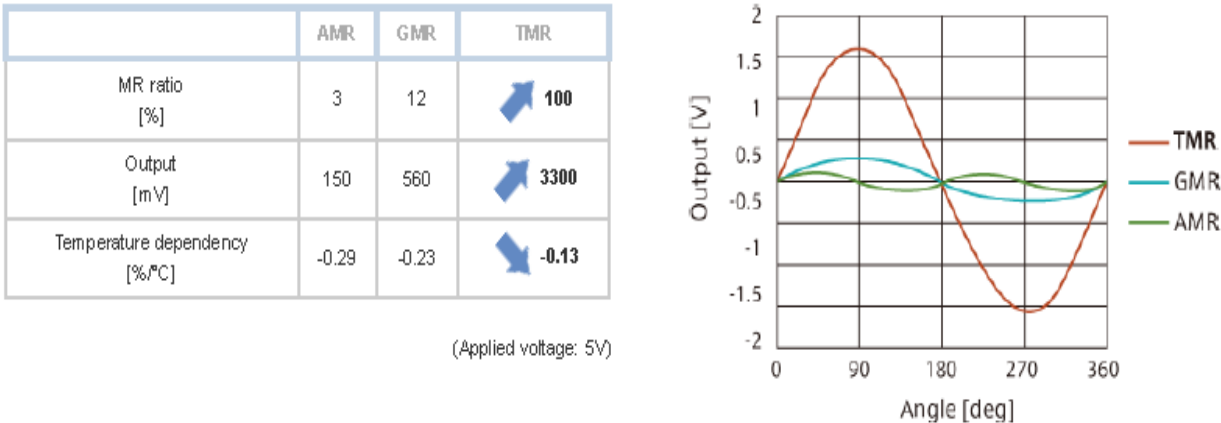
Fig 11 : Comparative analysis of the characteristics of magnetic sensors using a GMR element, AMR element and TMR element. [7]

Properties :

1) Low Power Consumption : The consumption of power for TMR sensor is 1/1000th of the Hall sensors and 1/100th of the AMR sensors, due to the high internal resistance of MTJ element.

2) Accurate detection : Although the performance of SQUID sensor is superior in terms of magnetic detection sensitivity, it has been proven that the thermal noise and the 1/f noise of MTJ element is possible to be reduced to 1nT/√Hz. This will help in implementing high space resolution and low cost for non-destructive test, low magnetic noise sensing and medical applications.

3) Range of operation : While conducting high-temperature tests, it has been confirmed that there is no diffusion of atom within the MTJ element even in temperature of over 150 º Centigrade. The TMR sensors are designed in such a way as compared to other sensors, that the sensitivity can be increased as the rise of temperature compensates the reduction of magnetic field in high temperature. Thus even in the range of high temperature, TMR sensor can detect a magnetic field, with the same air gap as in room temperature. The sensitivity of the TMR sensor is 10 times more as compared to AMR sensor and 3 times with respect to GMR sensor. The internal noise of TMR sensor is very small such that it can be used for measuring magnetic field of geomagnetism in the scale of µT.

4) Smaller in size : The MTJ element is different with respect to AMR and GMR element, since it makes use of electric current which flows vertically through the layers that compose the device. On improving the process of manufacturing such as the etching machining performance and side-etching performance, it is possible to significantly reduce the area of the sensor.
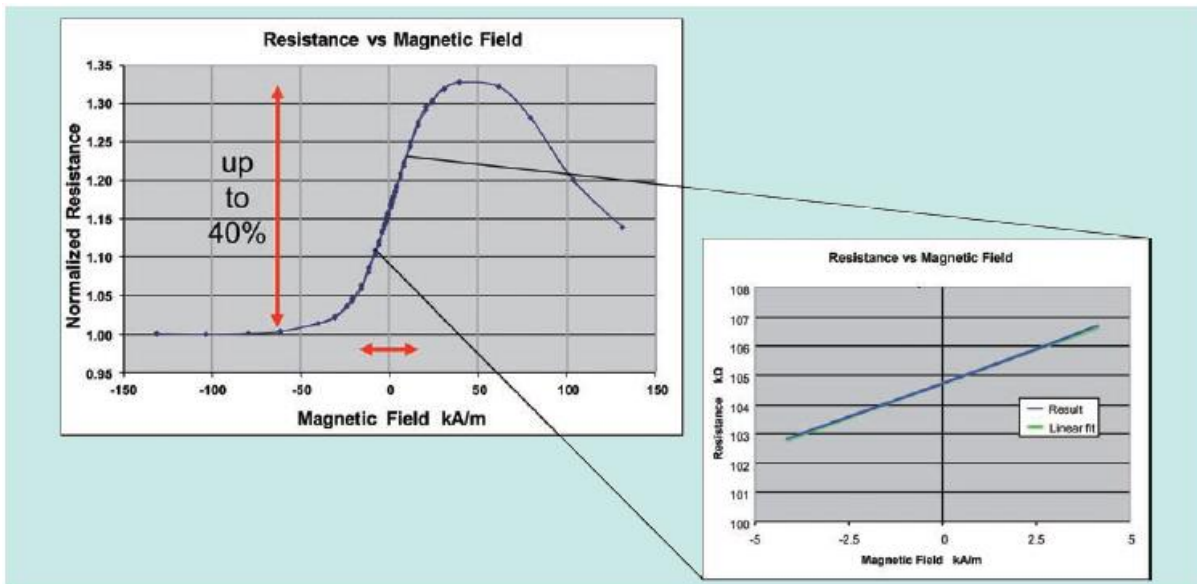
Fig 12 : Example of transfer curve for a TMR sensor with the following structure [7]

5) Electrostatic Discharge (ESD) resistance : The MTJ element can be considered as a structure comprising of a capacitor with a very thin nanoscale metric insulator which is susceptible to the risks of high insulation breakdown. While manipulating these sensors, special care has to be taken.

6) Tolerance against high magnetic field : It can be clearly seen in the Fig. 6, which exhibits that the resistance of the TMR sensor reverses under the influence of external magnetic field. Thus, this is the reason TMR sensor does not breakdown even under the influence of an external magnetic field produced by a rare-earth metal.

7) Large Signal Amplitude : The effect of TMR is very high as compared to other magnetoresistive (MR) technologies. Therefore the sensitivity of the sensor or the output of a sensor is much larger

4.2.2 Anisotropic Magnetoresistive Sensor (AMR)

Anisotropic Magneto-Resistive (AMR) sensors are contact-less and a precise device which measures the change in the angle of a magnetic field as sensed by the sensor. It is based on the property of Anisotropic Magnetoresistance , in which the electrical resistance depends on the angle between the orientation of the magnetic field and the direction of the electrical current. The discovery of the first magnetoresistive effect was made by William Thomson, in 1856, better known as Lord Kelvin. AMR sensors are comprised of nickel-iron or permalloy material in the shape of a thin film layer. The magnetization vector of this layer is in a specific direction and on the application of an external field to the layer, the vector rotates. Thus, depending on the magnitude and direction of the external field, the magnetization vector will deviate by an angle.
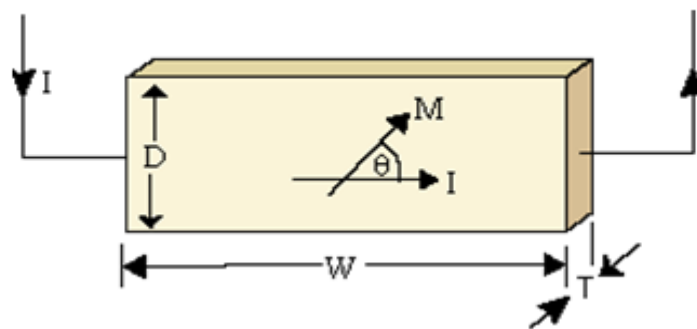
Fig 13 : The AMR effect observed in a thin film with single-domain state [8]

On the application of a strong magnetic field, the creation of magnetization vector takes place along the strip's length for magnetizing it, and then it is depicted in the Fig.5, where all the magnetic domains align together in a unique direction in the permalloy. Theoretically, this unique alignment will bring a change in the state of the magnetic domains in the thin film material, changing it to a single domain state.
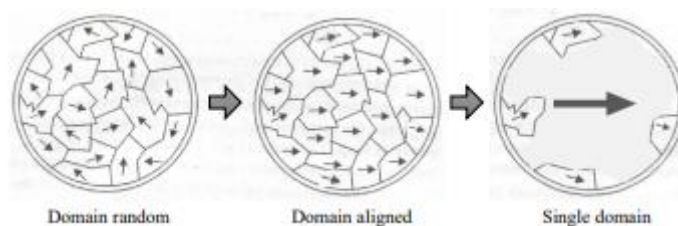
Fig 14 (a) : Magnetic field vector in AMR sensor[8]
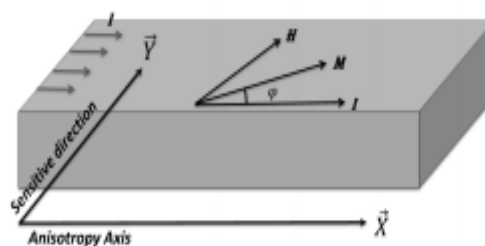
Fig. 14 (b) : Magnetization vector in AMR sensor[8]

In the Fig. 13, the AMR effect is described in a thin film in which the thickness is T, width is W, and depth is D with a single domain state as parameters of the film. The change in resistance in this thin element can be given as :

$$R = R_o + \Delta R \cos^2\Theta \qquad (4.5)$$

From the above equation, R_o represents the fixed part of the resistance while ΔR is the maximum change that can take place in the variable part of the resistance, which is also given as a function of angle in the Fig. 14.
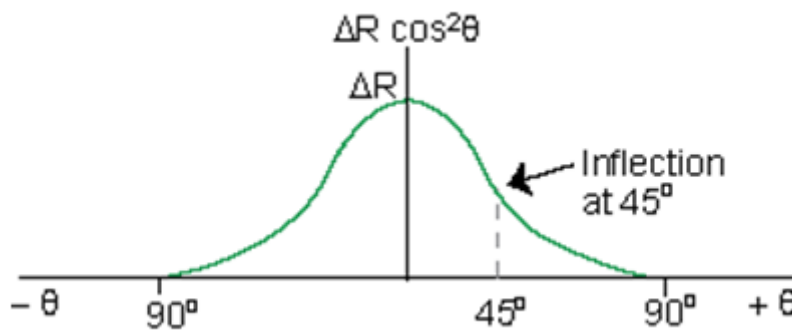
Fig 15 : Change in magnetization angle vs. the MR change in resistance [8]

In addition, it has been also shown in Fig. 13(b) that the output of the sensor depends on the angle between the anisotropy or easy axis direction and the magnetization vector (M). The sensor is surrounded by an external magnetic field (H), which modifies the angle by the rotation of the magnetization vector.
The relation between the external magnetic field and the angle could be found out, if the reference is made to the magnetic energy in a ferromagnetic layer by taking the single domain assumption into consideration (14). This equation is given as :

$$E = E_{mag} + E_{k} = -H.M + K_u \sin^2 \phi \qquad (4.6)$$

Where E_k and E_{mag} are the anisotropy and the magnetostatic energy, respectively. M represents the magnetization vector, H is an external magnetic field, K_u is the anisotropy constant and ϕ is the angle of magnetization vector with the anisotropy axis as shown in Fig.14(b).

4.2.3 Noise Sources for AMR & TMR

In this section, the different noise sources in MTJ and magnetoresistive sensors that originate from different mechanisms such as thermal electronic noise, shot noise, amplifier noise, 1/f noise and random telegraph noise (RTN) will be discussed. The noise sources have been studied and discussed in different other research papers before, and all these sources in MTJ sensors are incoherent in nature. Therefore, the total noise is considered as the non-coherent summation of these noises [37].

4.2.3.1 Amplifier Noise

The point or source of amplifier noise is not intrinsic to TMR & AMR sensor and it is created by the external conditioning circuit of the sensor system. The external amplifier is used to amplify the sensor output signal and the intrinsic noise of the amplifier degrades the sensitivity of the sensor system. Thus, the noise originating from amplifier is characterised and to meet the low noise requirements of the MTJ & AMR sensor, a low-noise amplifier should be used.

4.2.3.2 Shot Noise

Walter Schottky discovered this noise in vacuum tubes in 1918 and his work demonstrated the existence of a type of noise even if all the extrinsic noise sources were eliminated. The thermal effects causes discreteness of electrical charge and the stochastic nature of the electron emission process are associated with this fluctuating time-dependent phenomenon. Due to the uncorrelation of the emission events, the emission process of an individual electron from cathode is known as Poisson distribution. The fluctuations power density is given by :

$$S_I^{shot} = 2eI = S_{Poisson} \qquad (4.7)$$

Where I is the average DC current of current pulses and e is the electron charge. The contribution of both positive and negative frequencies are ideal and hence the use of factor 2. It had been found by different research groups that in MTJ & AMR sensors, the theoretical spectrum density value of shot noise calculated by Eq. (2.6) is not always equal to the practical value [38][39][40].

4.2.3.4 Thermal electronic Noise

Thermal noise is differentiated into two types of noises – thermal electronic noise , thermal magnetic noise depending on their origin. The later form of thermal noise is discussed later in this section. Thermal electronic noise was discovered by Johnson and Nyquist, who first reported this noise in 1928, hence the thermal electronic noise is also known as Johnson-Nyquist noise. This kind of noise appears in most contacting media and it occurs due to the random movements of charge carriers which are agitated by the variations in local temperature near Fermi level. Electrons gets energy from these variations which helps them to migrate across the barriers in conducting media and this migration phenomenon is also known as Brownian motion. In MTJ and Magnetoresistive devices, this noise is thermally induced and is considered as white noise. Johnson-Nyquist noise appears in both high and low frequency regimes.

4.3.4.5 Thermal magnetic Noise

The junctions of an MTJ device keeps on shrinking with the shrink of size of these devices. The magnetic fluctuations In MTJ devices starts dominating if the junctions are thermally activated. This type of noise is different from magnetic independent white noise, as it is field dependent. Investigation is being carried out on the origin of thermal magnetic noise, even though most researches suggests that it occurs due to the rotations of magnetization in the small volume of a free layer. At near

zero magnetic field, a certain form of noise was found to exist by Hardner et al. [41] which can be related to the defects found in the antiferromagnetic order in Cu/Co multilayers. Thermal magnetic noise is derived differently with respect to thermal electronic noise. It was suggested by Ingvarsson *et al.* [42] that the origin of thermal magnetic noise is due to electron hopping of domain walls between magnetic layers caused by thermal excitation. This theory was proved by Smith and Arnett [43] and it was also suggested that the nature of thermal magnetic noise is frequency independent and increases inversely with the free layer volume of MR sensors [37].

4.3.4.6   1/f Noise

In Magnetoresistive and MTJ devices, another important form noise source exists, which is the flicker noise or excess noise. It has been shown in a previous research that the current spectral density in different conductors or electronic devices, increases in an inversely proportional manner with respect to the low frequency domain [44]. 1/f noise differs from white noise on the note that it is frequency-dependent. At low frequency, the power spectral density is much larger than the thermal electronic noise and shot noise. In MTJ and Magnetoresistive devices, the 1/f noise can be characterized in two categories : the magnetic 1/f noise and the electronic 1/f noise.

- Electronic 1/f Noise :

  The source of electronic 1/f noise can be traced to trapping of charged electrons in barriers and in between interfaces of tunnel junctions [45] [46]. On the flow of current through the sensors, immobilization of some charges takes place at the defects in the barriers, which eventually slows down the mobility of carriers. Therefore the transmission processes of electrons , subsequently, disrupts each other. The highly crystallized tunnel barrier has been experimentally verified to serve two purposes – enhancement of TMR ratio and mitigation of the effect caused by 1/f noise in MTJ devices [47]. Enhancement in the quality of interfaces between thin films and reduced number of defects in the tunnelling barriers will be associated to this effect.

  The power spectrum level of the electronic 1/f noise is evaluated by the help of Hooge parameter , which is given by :

$$\alpha_{elec} = A f S_V^{elec,1/f} / V^2 \tag{4.8}$$

Where the power spectrum of the electronic 1/f noise is represented by $S_V^{elec,1/f}$, f is the frequency, A is the junction area, and V is the voltage across the junction. In order to parameterize the noise level of electronic 1/f noise, the Hooge parameter is used.

- Magnetic 1/f Noise

  Magnetic fluctuation is measured as well besides the electronic 1/f noise in the low frequency domain. The lower the frequency, the higher is the noise power spectrum of magnetic 1/f noise. The magnetization alignment switching status at the interface between free layer and pinned layer is ascribed to this magnetic fluctuations. This kind of magnetic fluctuation is different with respect to the one induced by external magnetic field. It represents the noise evoked in the direction of internal magnetization.

.4.3.4.7   Random Telegraph Noise (RTN)

Random Telegraph Noise was invented by Kandiah and Whiting in 1978 when they were systematically studying double-gated junction field-effect transistors (JFETs) [48]. The researchers had found that RTN was generated due to a defect , center of charging and discharging process. After elimination of the magnetic noise in MTJ devices, by the saturation of junctions with external magnetic field, it was observed in low frequency regime that RTN interwines with electronic 1/f noise and it became more highlighted when the biasing current was increased [49]. Its only applicable for MTJ devices.

4.2.4 Other Magnetic Sensors

While both magnetoresistive and hall-effect sensors measures the strength of magnetic field components, but they do so in a different way. Hence, in order to choose the sensor better for the purpose, its better to check the sensor characteristics. One of the main purpose of the LISA mission is to detect GW waves in space in the low frequency domain of 0.1mHz − 1Hz. In order to detect magnetic fields in this range, we need to find the right fit sensor, based on certain parameters such as power consumption, sensitivity, dynamic range, intrinsic noise, resolution, size and temperature performance.Atomic magnetometers are also magnetic sensors that are based on NMOR technology with modulated light at sub-millihertz frequencies. Previously, work has been done using atomic magnetometer[16] in a signal conditioning circuit and it was found that the noise estimation was conforming with the LISA measurements and therefore it is a promising technology for the LISA mission due to its functioning at 0.1 mHz and the measurements being taken are dominated by 1/f noise at low frequencies. However, the sensitivity of atomic magnetometer is extremely high at 0.1 mHz. But, due to the weight, size and power restrictions for its application in space, further work has to be carried out in miniaturization of these sensors.
Therefore, it rules out the possibility of using it for LISA mission. Giant magnetoimpedance (GMI) sensors comes in the form of thin ribbon, or wire which is supplied by high frequency current. The change of impedance occurs due to either skin effect or dependence of permeability on external constant field [50]. Thus, the change of impedance is massive for relatively small magnetic field. The power consumption of GMI is as low as $5 * 10^{-3} \ W$. Extraordinary magnetoresistance (EMR) is another magnetic sensor which potrays extremely large magnetoresistive effect that is present in special heterostructure comprising the metal shunt and semiconductor. However, the sensitivity of EMR sensor is small and they need several orders of magnetic field [50]. Hence, it cannot be an option for a magnetometer pertaining to LISA mission.

On miniaturising the sensor size, the overall noise increases.Proton magnetometer is another type of magnetic sensor, and it is also known as proton precission magnetometer (PPM) and it makes use of the Earth's field nuclear magnetic resonance (EFNMR) for measuring small variations in the magnetic field of Earth, allowing ferrous objects on sea and land to be detected [51]. It is generally used in land based archaelogical business, and detecting wrecked ship in the sea, but, this magnetometer is big in size and hence it cannot be used in LISA mission. MR based sensors such as

GMR and AMR provides promising characteristics especially when size is a limitation. However, the range, noise performance and linearity of AMR and TMR is far better than GMR. SQUID magnetometers are huge and even though they have higher range of sensitivity and low noise but they are bigger in size and it can only operate in cryogenic temperature and therefore it is impossible to be used for such a space mission [50]. Hence, these magnetometers does not qualify to fulfil the requirements of the LISA mission.

4.2.5   Noise performance of the magnetic sensors (AMR & TMR)

On enhancing the sensitivity of TMR sensors, the intrinsic noises strongly deteriorates the measurement sensitivity of the sensor while it limits the signal-to-noise ratio (SNR). The SNR can be enhanced by eliminating the noises in TMR sensors. Hence, analysis of the theoretical and experimental noises in TMR and AMR sensors are really important for optimizing the performance of these sensors. The different sources of noise in TMR and AMR have been previously discussed. The behaviour of power spectral density at low frequency of all these sources can be modelled by :

$$S_B(f) = \ S_{wn}(1 + \frac{f_c}{f^{\alpha}}) \tag{4.9}$$

Where Swn stands for the white noise of the TMR, the corner frequency fc tends to be higher than 1 Hz and the value of α is generally 1. In our application as a space based magnetometer, the last two terms are of great importance along the milli-hertz range. The instrument noise is also taken into account which is described by root-mean square (rms) noise power, that is obtained by integrating the power spectral density over a given bandwidth from fH to fL. In the case, where the value of α is 1, the mean square of the noise is given by :

$$B_{n,rms}^2 = \ \int_{f_L}^{f_H} S_B(f) df = S_{wn}(f_H - f_L + \ f_c ln \frac{f_H}{f_L}) \tag{4.10}$$

The model prediction of the noise of the sensor is based on the semi-empirical equation (2.6) only able to solve with an approximate solution and it is meant for spectra at frequencies below 1 Hz. Therefore, a test was conceptualised for characterising the low-frequency noise, and in accordance with Eq.(2.1), verify whether the system (comprising the magnetometer along with its associated electronics) will be able to ascertain the magnetic fluctuations of 10nT/√Hz down to 1mHz.

During the experiment, the stability of the external ambient field is affected by the Earth's magnetic field variations and environmental perturbations due to the equipments in the laboratory. Hence, due to the fact that the amplitude spectrum of the environmental magnetic fields in the laboratory is around 200 nT / √Hz at 1 mHz, therefore the sensor noise measurements are required to be performed in appropriate conditions of magnetic cleanliness. The value of these variations are reduced to a number lower than 1nT / √Hz at a frequency of 1mHz for discriminating between the true environmental fluctuations and the noise of the system. Therefore, in other words, the external ambient field is necessarily shielded at a level better than the value 46dB, which can be easily obtained by the means of a passive enclosure of a material with high-permeability. The shielding factor is represented by :

$$A_{db} = 20log_{10}\frac{B_{out}}{B_{in}} \tag{4.11}$$

Where Bout represents the external magnetic field before the shield is placed, and due to Bout, the residual magnetic field inside the shielding is given by Bin. Therefore, the magnetometer that was going to be tested was placed inside a three-layer cylindrical enclosure of mu-metal (nickel-iron alloy) for screening out the slow drift of the environmental magnetic field, which occurs due to the inverse power-law frequency dependence of the magnetic field of the Earth. All the runs that were made in measurements were allowed to run for atleast five hours, which is enough in order to estimate the amplitude spectral density (ASD) at 1 mHz.
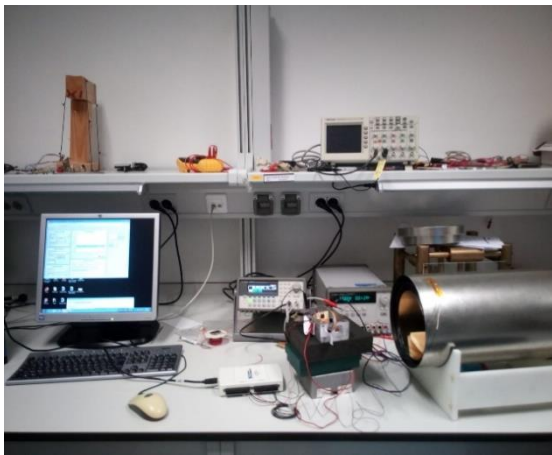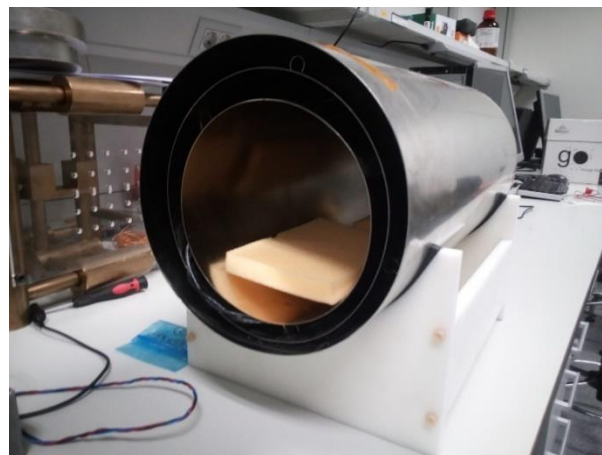
(a)   (b)

Fig 16 : (a) This is the total experimental setup for testing the TMR & AMR sensor. (b) It is the shielding made of 3 mu-metal cylinders which screens out the environmental magnetic field.

 In order to determine the noise performance of the system , the procedure was split into two parts, the noise measurements of (1) the sensor to be used plus the signal conditioning circuits, and (2) the circuits utilised for the Data Acquistion Unit (DAU). The noise of the circuit is measured by short circuiting the signal conditioning circuit and replacing the sensor in the circuit with a wheatstone bridge configuration of resistances, thus the data acquired by the ADC would be the noise of the signal conditioning circuit minus the sensor. Another noise measurement is done alongwith the sensor plus the signal conditioning circuit. Therefore, when the noise of the signal conditioning circuit is subtracted from the noise measured with the configuration of the sensor plus the signal conditioning circuit gives us the noise of the sensor.

This noise floor, that exceeds the noise level measured by the magnetometer, gets limited by the sampling frequency that is imposed by the spacecraft telemetry. The low frequency measurements are dominated by 1/f noise of the sensor curves and the low-frequency noise levels are essentially the same (~ 0.8nT/√Hz at 1mHz). However, at higher frequencies, discrepancies have been by white noise, between the different axes by a factor of three. The deduction that can be made from this possible discrepancy can be the existence of a higher residual field more than expected or the proximity of electronics in the vicinity of the y-axis of the magnetometer that can create

magnetic disturbances .Therefore, as a whole, three magnetometers were tested. The results of the experiments that have been made regarding noise characterisation has been reported and discussed later in the thesis.

4.2.6 Commercial magnetic sensor

4.2.6.1 TMR9112 magnetometer

The TMR9112 is a Tunneling Magnetoresistive (TMR) sensor which is being manufactured by MultiDimension Technology. They are basically magnetoresistive Wheatstone bridges configured to measure magnetic fields in a reliable way after it is exposed to large magnetic fields or experiencing extreme temperature drift, which can be powered using a current or voltage supply. On the application of power, the magnetoresistive Wheatstone bridge converts any magnetic field applied along the sensing axis direction to a differential output voltage. The TMR9112 comprises of an initialization coil which is magnetically coupled to the TMR sensor, in addition to the magnetoresistive bridge circuit. This is a feature that is patented by MultiDimension which permits proper magnetic alignment, even in an uncontrolled environment where temperature change or large magnetic field exposure cannot be avoided, which results in a sensor which will be able to provide low offset output and stable low hysteresis. The packaging of TMR9112 sensor is made in a 6mm X 6mm X 0.75 mm LGA assembled package which can be seen in the following Fig. 7.

(a)   (b)
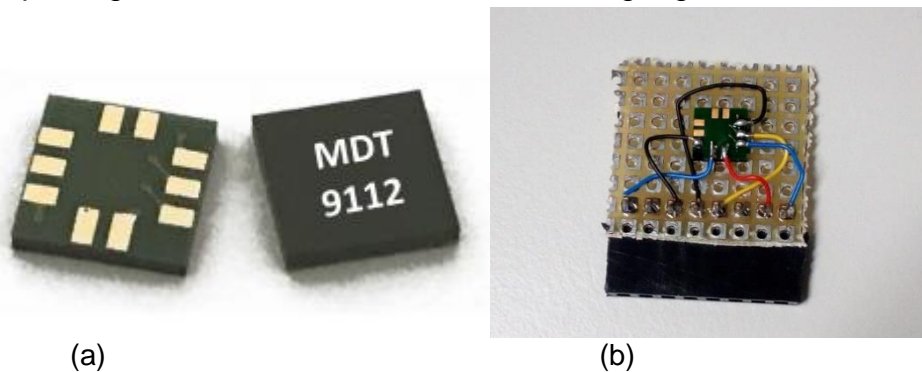
Fig. 17 : (a) TMR9112 sensor assembled in a 6mm X 6mm X 0.75 mm package[13] (b) TMR9112 sensor connected to the signal conditioning circuit used for testing this sensor

Transfer Curve :

The figures displayed exhibits the response of the TMR9112 sensor to an applied magnetic field in the ranges +1 & -1 Oe and +10 & -10 Oe when this sensor is biased at 1V. While operating in a field less than 10 Oe, the coercivity will remain small, eliminating the need of the initialization coil.
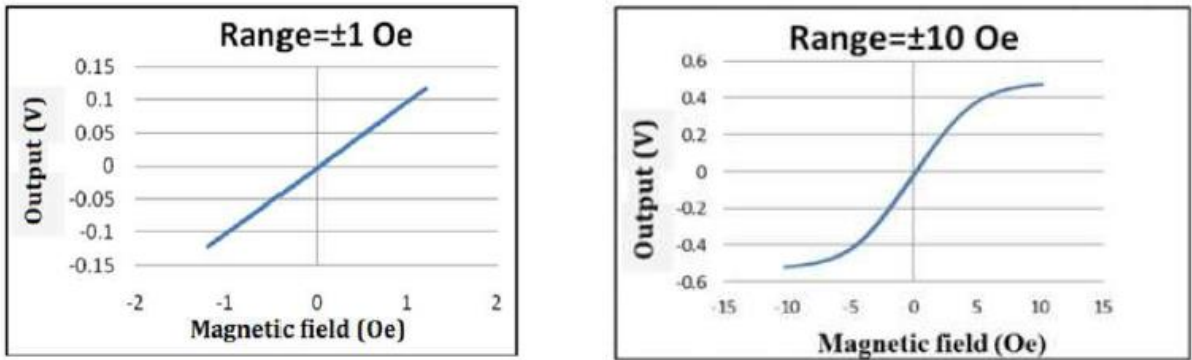
Fig 18 : Transfer curves of TMR9112 sensor in the ranges +1 & -1 Oe and +10 & -10 Oe[13]

Table 4.1 : Performance Specifications (Vcc = 1.0 V, Ta = 25 ⁰C) [13]

Parameter	Symbol	Conditions	Min	Typ	Max	Unit
Supply Voltage	V_{cc}	Normal Operating		1	7	V
Supply Current	I_{cc}	Output Open		20[2]		µA
Resistance	R			50		kOhm
Sensitivity	SEN	Fit ±1Oe		100		mV/V/Oe
Saturation Field	H_{sat}			±8		Oe
Non-Linearity	NONL	Fit ±1Oe		0.5		%FS
Offset Voltage	V_{offset}			15		mV/V
Hysteresis	H_c	Sweep ±1 Oe, Fit ±1 Oe		0.02		Oe
High Field Hysteresis	HFH_c	Sweep ±150 Oe, Initialization		0.05		Oe
Equivalent Magnetic Noise Density	S_B	@1Hz		150		$pT/\sqrt{Hz}$

Notes :

1. 1 Oe (Oersted) = 1 Gauss in air = 0.1 mT = 79.8 A/m
2. ICC = Vcc / R, Icc will vary with different R, and it can be customized accordingly.

Table 4.2 : Initialization Coil parameters

Parameter	Symbol	Conditions	Min	Typ	Max	Unit
Resistance	Rcoil		0.6	0.8	1.0	ohm
Current	Icoil	<10 µs current pulse, 0.1% Duty Cycle		2	5	A
Resistance Tempco	RTC			0.393		%/C

Sensor Equivalent Magnetic Noise :

The following figure portrays the Power Spectral Density (PSD) of the intrinsic noise of the TMR9112 sensor with reference to the magnetic field. The 1/f noise given by the manufacturer of this sensor is approximately 150 pT/√Hz @ 1 Hz, and the value of white noise is approximately 4.5 pT/√Hz @ 10 Hz.
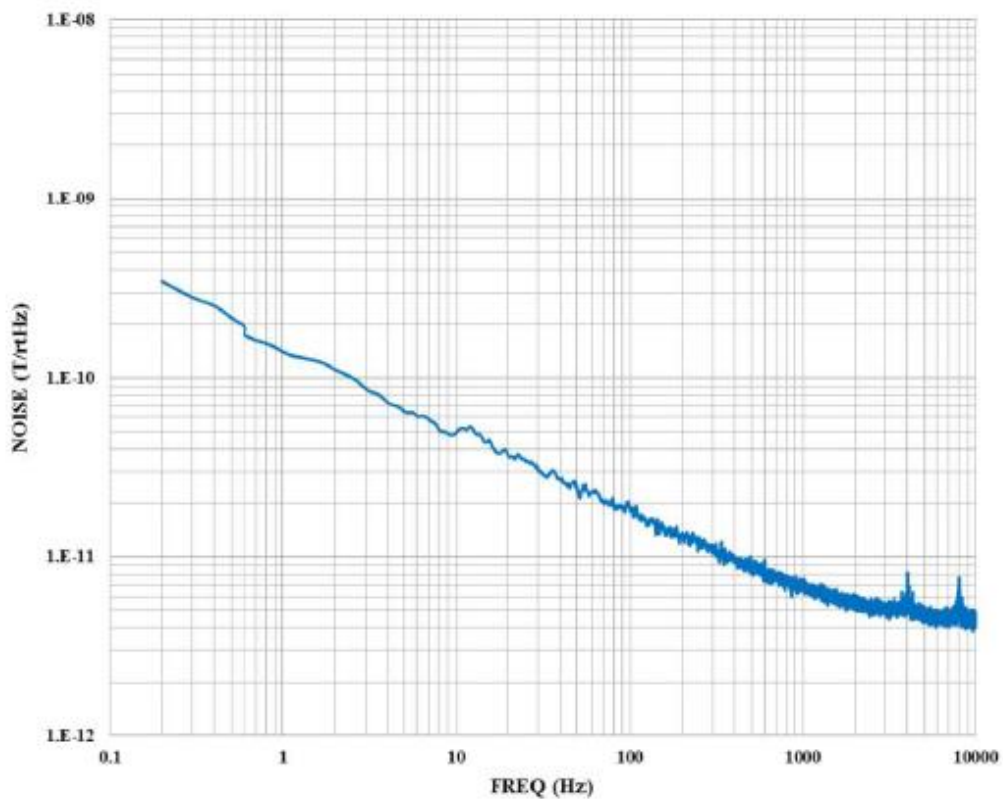
Fig. 19 : Power Spectral Density (PSD) of the intrinsic noise of the TMR9112 sensor wrt magnetic field as given by the manufacturer. [13]

Sensor Initialization

The sensor magnetic initialization is performed by a coil that is provided within the sensor package, after the sensor has been exposed to a large external magnetic field or under other circumstances that can cause demagnetization of the sensor, such as change of temperature or stress.

On a general basis, the performance of magnetic sensors, such as giant magnetoresistance (GMR) , anistropic magnetoresistance (AMR) as well as TMR depends on the temperature, magnetic field, and stress exposure history. When external large magnetic fields are applied along the sensing direction, the sensor produces hysteresis values larger than small fields, and it can produce a shift in calibration of the device and offset by demagnetizing the ferromagnetic materials used in the sensor. The source of these large external magnetic fields can be permanent magnets placed near the sensor, transformers and current spikes in power cables, etc. Application of a stress or change in temperature on the sensor package can demagnetize the sensor elements. This demagnetization due to such sources does not destroy the sensor, but it can shift the operating parameters. The sensor accuracy of TMR9112 can be affected due to magnetic fields greater than 10 Oe. The normal operating condition can be restored by the application of a quick large magnetic field pulse along the direction perpendicular to the sensing axis. A simple low power method is provided by the initialization coil , for initializing the sensor back to the magnetic condition, thereby restoring the normal operation of the sensor.

4.2.6.2 CT219 Series magnetometer

The CT219 Series is a differential current sensor based on the patented TMR technology of Crocus Technology, i.e , the Magnetic Logic Unit™ (MLU™), especially designed for industrial and consumer applications. The CT219 sensor is used in a closed loop circuit configuration , in order to measure bi-directional magnetic fields which is being generated by a current carrying conductor such as a bus bar or PCB trace. This sensor provides high sensitivity with a design flexibility in a small footprint SOT-26 package and this technology is economic and available at a competitive cost due to high volume manufacturing.

Fig 20: Crocus Technology CT219 series sensor [53]

Table 4.3 : The absolute maximum ratings of the CT219 series sensor [53]

Parameter	Symbol	Min	Max	Unit
Supply Voltage	Vs		10	V
Supply Current	Is		300	uA
Operating Temp	Ta		125	°C
Storage Temp	Ts		150	°C
Soldering Temp	T		260	°C
Magnetic Flux Density	B		1	T

Table 4.4 : The electrical characteristics (Supply voltage = 5.0V, Ta = 25º C) are displayed in the given table. [53]

Characteristic	Symbol	Conditions	Min	Typ	Max	Unit
Operating Temperature	Ta		-40	25	85	°C
Supply Voltage	V_B			5		V
Supply Current	I_B				200	µA
Quiescent Voltage	Vo	B=0, I_u= 5mA	2.3	2.5	2.7	V
Input Bias Current	I_u			5		mA
Field Line Resistance	R_{lu}	Each Resistor		30		Ohm
Sensitivity				75		mV/mT
Linearity Error*		±1.0 mT		0.5	1.0	%FS
Hysteresis		±1.0 mT		1		%FS
Operating Frequency*					1	MHz
Temperature Coefficient of Output*				15	30	ppm/°C

Fig. 21 : Performance characteristics typical to the CT219 sensor as given by the manufacturer[53]
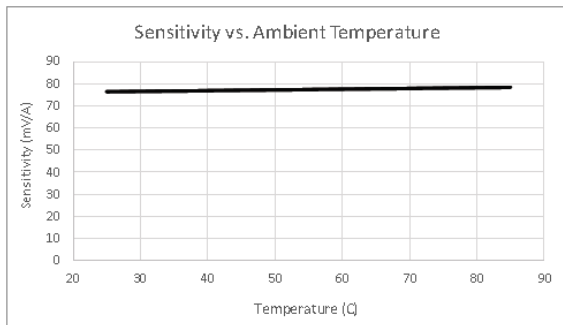
Note: Sensitivity based on current trace measurement on PCB
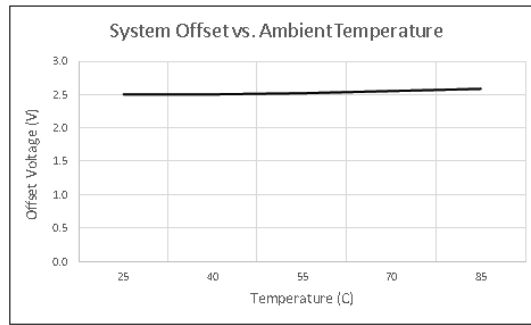
Note: Sensitivity based on current trace measurement on PCB
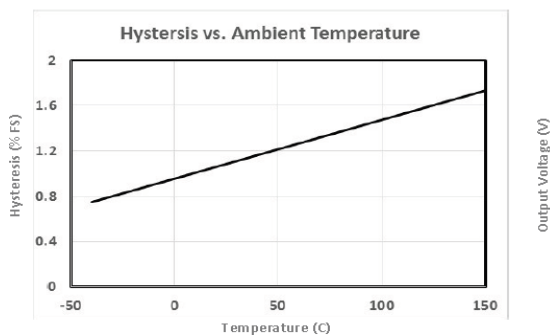
4.2.6.3 HMC1001/1002 magnetometer

The Honeywell HMC1001 and HMC1002 are one axis surface mount magnetic sensors, specifically designed for low magnetic field sensing. This cost effective sensors are supported by signal processing and encompassing solutions are enabled. These low cost and small sensors are great solutions , as they are easy to assemble for high volume OEM designs. The application domain of these two sensors comprises navigation systems, magnetometry, current sensing, and compassing.

The HMC1001 and HMC1002 sensors utilises Honeywell's AMR technology (Anisotropic Magnetoresistance) which provides several advantages over coil based magnetic sensors. They are solid state magnetic sensors, high-sensitive, low field which are designed to measure magnitude and direction of earth's magnetic fields in the range of micro-gauss to 6 gauss. These sensors manufactured by Honeywell are the most sensitive and low field magnetic sensor in the industry.
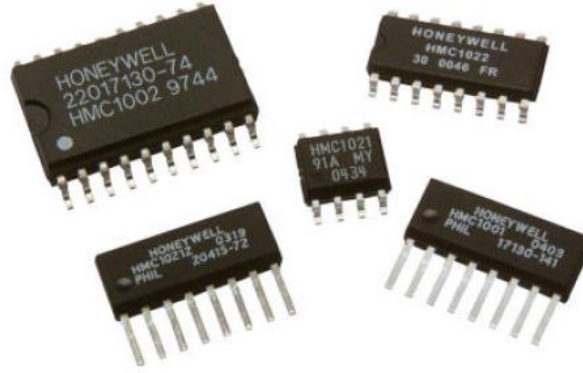
Fig 22 : Honeywell's HMC1001 & HMC1002 magnetic sensors [52]
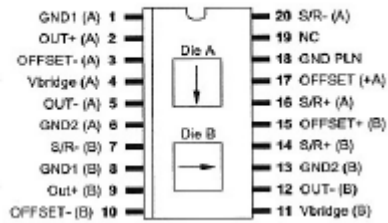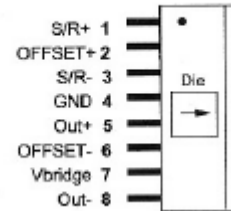
Fig 23 : Package / Pinout Specifications of the HMC1001/1002 [52]

The noise density curve of the AMR HMC1001/1002 sensors are given in the figure below. The 1/f slope of the curve has a nominal slope of frequency near 10Hz and flattens out to a 3.8 nV/sqrtHz slope. This is an approximate value which is equivalent to the Johnson noise(also called white noise) for an 850 ohm resistor, that is the typical resistance. In order to understand the relation between noise density voltage and magnetic field , we use a couple of expressions such as :
Therefore Vbridge = 5V and Sensitivity = 3.2 mV/V/gauss, the bridge output (Voutput) is given by 16mV/gauss.
The noise voltage density at 1Hz is around 30nV/sqrtHz. In order to convert it to magnetic field , it has to be divided by the sensitivity of the sensor (T/V)
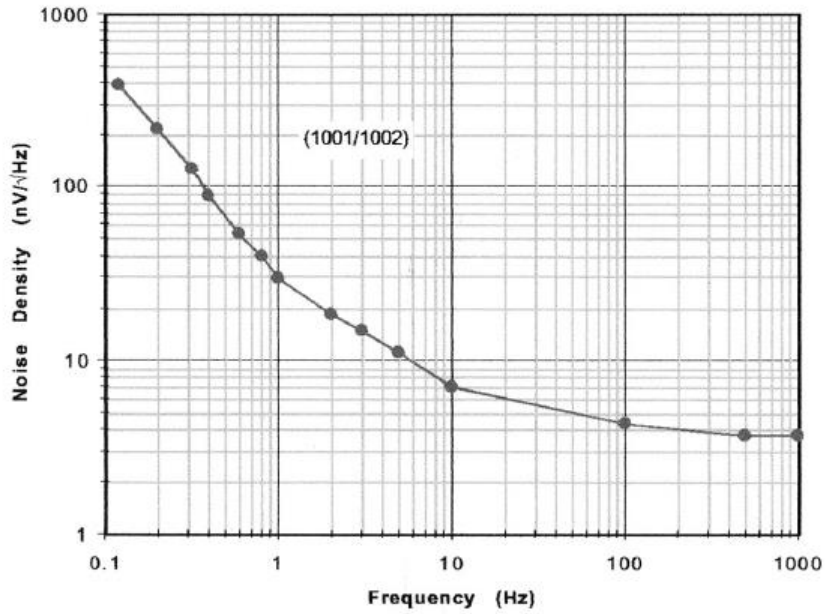
Fig 24 : Noise density curve of HMC1001/1002 AMR sensor given by manufacturer[52]

Table 4.5 : Comparative Analysis of Parameters of Solid State Magnetic Sensing
Technology:

Parameter	Hall Effect	AMR	GMR	TMR
Power Consumption (mA)	5-20	1-10	1-10	0.001-0.01
Die Size (mm²)	1 X 1	1 X 1	1 X 2	0.5 X 0.5
Field Sensitivity (mV/V/T)	~ 0.05 x 10^{-4}	~ 1 x 10^{-4}	~ 3 x 10^{-4}	~ 100 x 10^{-4}
Dynamic range (µT)	~ 10^{6}	~ 10^{3}	~ 10^{4}	~ 10^{5}
Resolution (nT/√Hz)	>100	0.1 ~ 10	1 ~ 10	0.1 ~ 10
Temperature Performance (ºC)	<150	<150	<150	<150

The different commercial sensors that have been used for this thesis are
HMC1001/1002, TMR9112 and Crocus CT219 series. A comparative analysis have
been made with the respective information being taken from the application note of the
sensors.

35

Table 4.6 : Comparative Analysis of Parameters of Commercial Magnetic
Sensors[13][52][53]

Parameter	TMR sensor (MDT)	TMR sensor (Crocus Technology)	AMR (Honeywell, HMC1001/2)
Die Size (mm²)	6 X 6	2.90 X 1.60	12.90 X 7.417
Sensitivity (V/T)	2500	75	160
Temperature Performance (ºC)	-40 to 125	-40 to 125	-55 to 150
Linearity error (%FS)	0.5	1.0	0.05 (+/-1 Gauss) 0.4 (+/- 3 Gauss) 1.6 (+/- 6 Gauss)
Supply Voltage (Volts) (Typical)	1	5	5
Bridge offset (mV)	15		-15
Typical Noise Density (@1Hz) (T/√Hz)	$1.5 * 10^{-10}$		$1.85 * 10^{-10}$

4.3 Noise Reduction Techniques

The noise characteristics intrinsic to the sensor that is specified by the manufacturer does not comply with the requirements. In order to make the noise characteristics compliant with the mission requirements, electronic noise reduction techniques have been employed to minimize the noise level of the sensor in the LISA frequency band. This section describes the methods that have been studied.

4.3.1 Flipping

One of the most promising noise reduction technique for reducing noise in magnetoresistive sensors is flipping. Anistrophic Magnetoresistive sensors (AMR) include a thin film which is made of a nickel-iron alloy with magnetic anistrophy. These sensors consists of an axis aligned with the sensor magnetization known as the easy axis while it also have a sensitive axis in the direction of the magnetic field, called the hard axis. The flipping mechanism takes advantage of these properties of AMR and it causes the internal magnetization of the sensor strips , to periodically flip, by the application of set/reset pulses implementing switching mechanism. This switching field pulses are generated by means of a thin film conductor, which is wound around the

active area of the sensor [54]. The output characteristics are reversed when there is a change in the direction of magnetization, and as a result, the output signal of the sensor is modulated at the frequency of set/reset pulses. It is followed by measurements of the magnetic field between each reset and set pulses, which are subsequently demodulated. The bridge offset and the associated temperature dependence can be subtracted using this sequence, due to the unchanged value of the offset voltage while the sensor output causes reversal of the polarity. Figure 25 exhibits the opposite slopes in the output characteristics after the application of the switching field pulses, and the following extraction of offset voltage for different values of bridge voltages. One of the main advantages of performing modulation techniques by the use of flipping pulses, is the reduction of 1/f noise within the required bandwidth. Another significant advantage is recovering degraded output signal which is induced by strong external magnetic fields (> 300 µT).
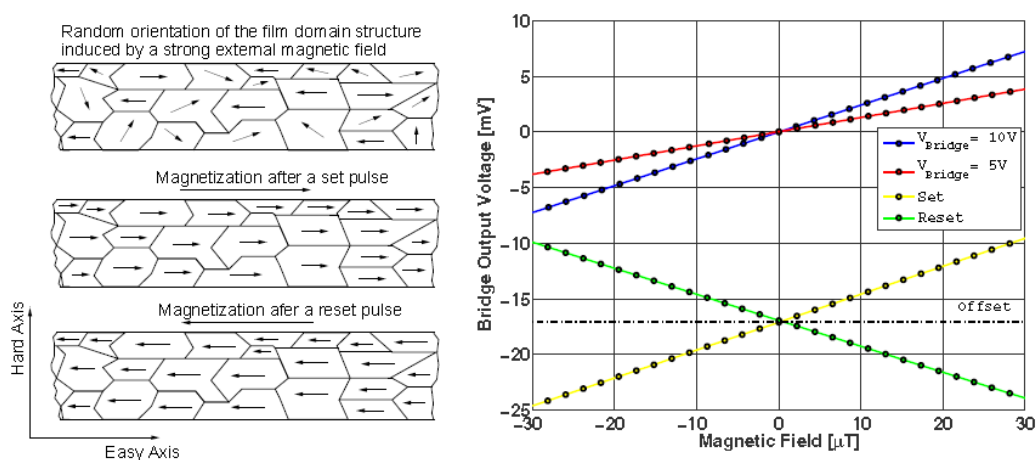
Fig 25 : AMR sensor response to the flipping mechanism. Left : magnetic alignment of the permalloy thin film domain structure using reset/set pulses. Right : output characteristics as a function of the magnetic field after a set (yellow trace) and reset (green trace) pulse with Vbridge = 10V. The extraction of bridge offset is done for Vbridge = 10V (blue trace) and Vbridge = 5V (red trace) [16]

The flipping technique does not work for TMR sensor as it does not have switching pulses and change of polarity. Hence it is not applicable for MTJ based sensors.

4.3.2 Electromagnetic Feedback

The coupling between magnetic field output and temperature can be reduced, by actively compensating the thermal dependence during its operation cycle. While taking measurements, the drifts in temperature will show up as error in gain. Hence, a feedback controller is used to maintain the bridge output close to zero, which reflects balanced bridge condition, thereby reducing thermal effects. On employing electromagnetic feedback, an opposing field is induced by an integrated coil which is associated in the closed-loop controller, for counteracting the field component detected by the sensor. The magnitude of the magnetic field measurement will be given by the flow of current through the compensation coil along with the current-to-field conversion of the coil. This method is used particularly at low frequency measurements where drifts in temperature is highly significant in the overall noise of the sensor.

37

4.4   Front – End Electronics

4.4.1   Working Theory

Anisotropic Magnetoresistor sensor or AMR is a magnetometer which comprises of a core containing Wheatstone bridge that is made up of four magnetoresistors with a structure of Barber-Poler for getting a linear output. Therefore, the resistance – magnetic field of the AMR can be expressed as :

$$R_{AMR} = R_{b,n} + \Delta R \frac{B_m}{B_o} \sqrt{1 - (\frac{B_m}{B_o})^2} \tag{4.13}$$

And in this equation $R_{b,n}$ is the nominal resistance of the magnetoresistive element, ΔR potrays the maximum change of resistance in response to the magnetic field, B_m is the field being measured that is perpendicular to the easy-axis, and the total anistropic field is given by B_o, which is determined by the geometry and material of the sensor. Subsequently, the output voltage of the Wheatstone bridge with four identical magnetoresistive elements that varies in opposite directions is shown by :

$$V_0 = V_b \frac{\Delta R}{R_{b,n}} * \frac{B_m}{B_0} \sqrt{1 - (\frac{B_m}{B_0})^2} \tag{4.14}$$

Where the bridge excitation voltage is V_b. The signal received at the output of the Wheatstone bridge is low-pass filtered, amplified, sampled and digitally demodulated. The analog signal conditioning circuit for sensing magnetic field using AMR with the flipping method in shown in Fig.25 [3].
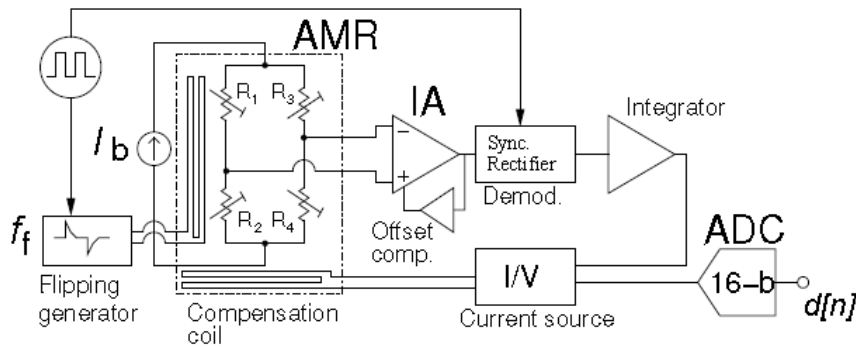

Fig. 26 : Analog signal conditioning circuit with AMR sensor for the flipping method alongwith electro-magnetic feedback [16]
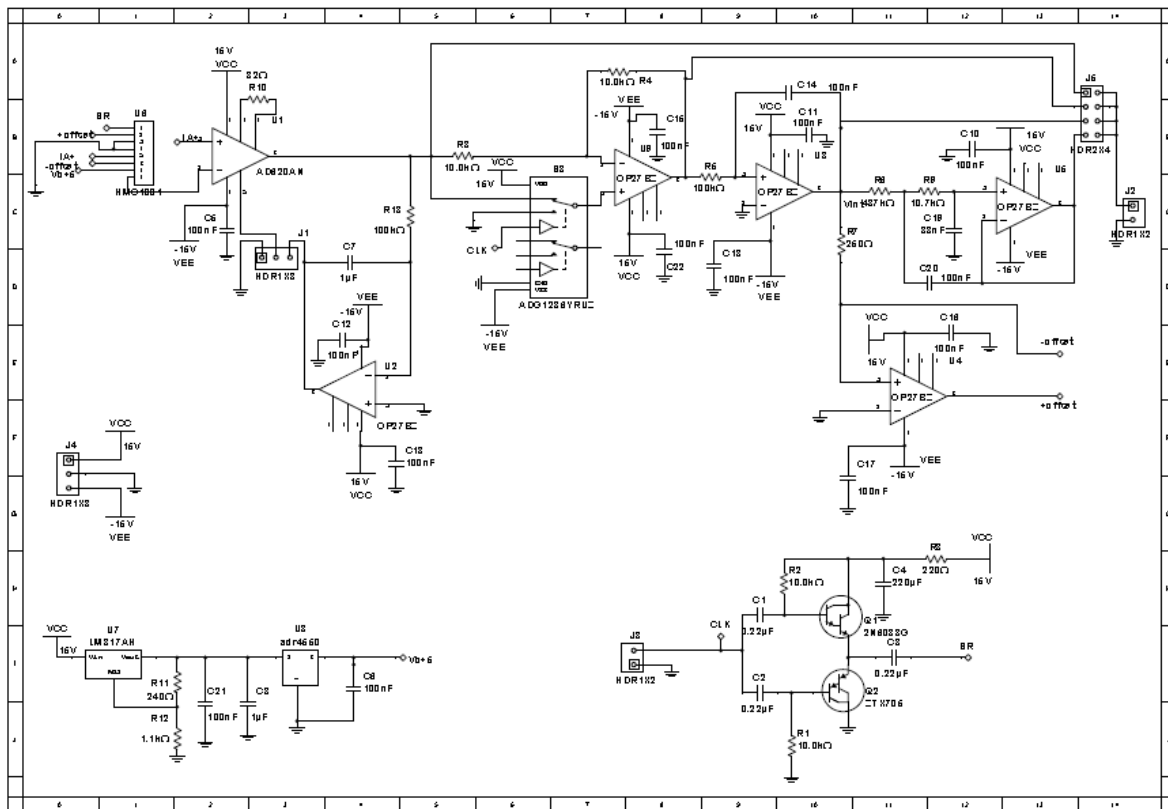
Fig 27 : Schematics of the AMR signal conditioning circuit

The circuit developed for flipping generator generates short reset/set pulses along a strap of 1.5Ω integrated in the sensor with peaks at 3.3A [3]. Although the circuit delivers peaks of high current and since the pulse duration is so short that the quantity of energy originating from the charged up capacitor is really small ($E = 0.5\ CV^2 = 2.75$ μJ for $C = 0.22\ \mu J$), see Fig. 25 for further details. The flipping frequency f_f has been set to 10 Hz, performing a modulation of the signal from the magnetometer at a frequency high enough to be outside the 1/f noise of the instrumentation amplifier (IA). The frequency that has been chosen for performing modulation on the signal is a trade-off among the effects on the thermal and magnetic disturbances that is produced by a more periodic switching signal, 1/f noise reduction, and the transient response after the pulses. Measurements of the magnetic field are acquired 10ms after every reset and set pulses, so that the flipping currents have died down below the micro-ampere level, and the low-pass filter settling time has elapsed. This avoids any glitches and transients at the input of the analog-digital converter.

The circuit (see Fig. 25) also includes an electromagnetic feedback mechanism , which comprises of a current regulator that feeds the compensation coil with the measured magnetic field. The sensor output signal is forced to zero with the help of an integrator in the control loop for removing the remaining error. The magnitude of the measured field is shown as voltage at the output of the integrator, that is proportional to the compensation current.

The TMR sensor comprises 4 magneto-resistors forming Wheatstone bridge as in the AMR.

39
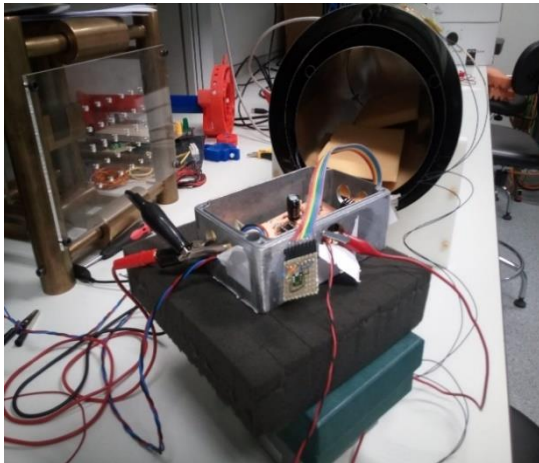
(a)
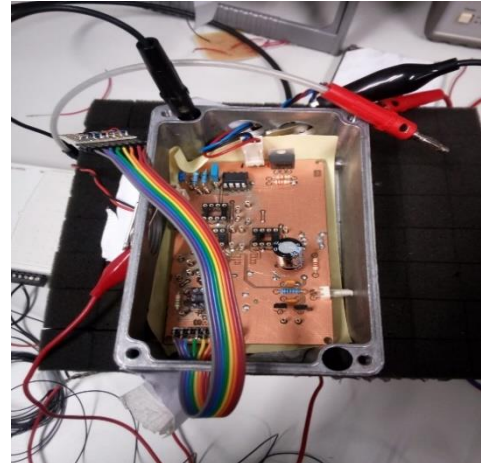
(b)

Fig 28 : (a) (b) This shows the experimental setup containing the front end electronics and the PCB circuit designed for testing the TMR sensor. The sensor attached to the signal conditioning circuit with the help of a tape is placed inside the mu-metal shielding in order to shield the environmental magnetic disturbances.

Fig 29 : Schematics of the TMR signal conditioning circuit

The main differences with respect the AMR are:
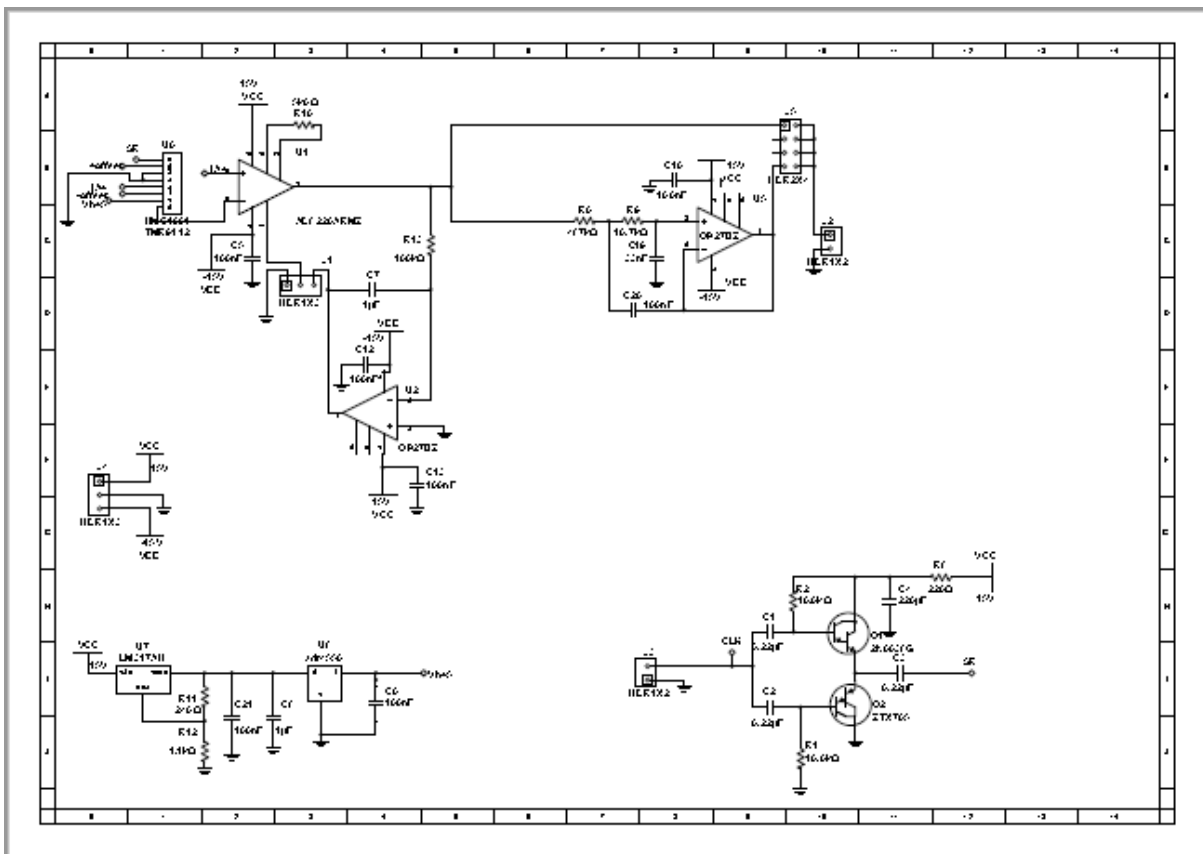
-The resistance of the bridge is in the order of 50 kΩ compared with the 840 Ω of the AMR. This reduces significatively the power consumption but increases the sensitivity of the circuit to external interferences.

-The sensitivity of the sensor is 2000 V/T compared to the AMR 160 V/T. Thus, the gain of the IA has to be lower.

-The init pulses do not reverse the polarity of the sensor. It is not necessary for using a synchronous rectifier.The pulse circuit can be the same of the AMR.

-The sensor does not have a feedback coil to work at zero field. The circuit for the feedback coil has been removed.

Considering all these differences the simplified block diagram of the signal conditioning circuit for this sensor is in figure 26.
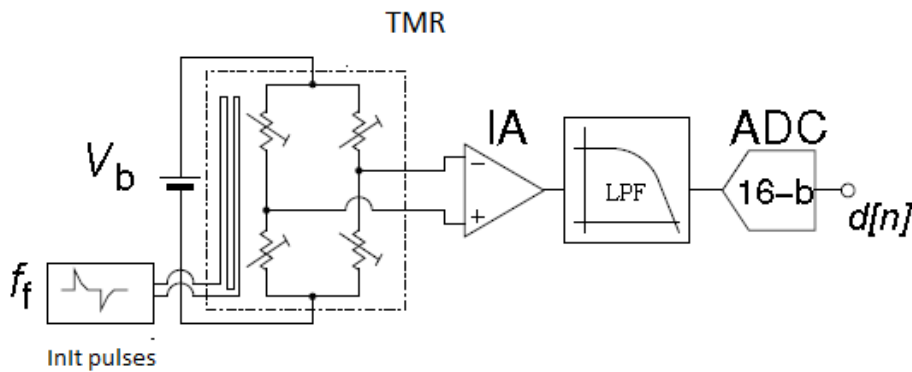
Fig 30 : Analog signal processing circuit with TMR sensor using Init pulses

The magnetoresistive sensors that are manufactured are often quoted with a hysteresis specification as a percent of full scale applied magnetic field. Therefore, to decrease the impact of this intrinsic hysteresis issue in MDT TMR sensors, these sensors uses a method to apply Init Pulses for making their response independent of magnetic field history. The MDT TMR9112 sensor uses Init Pulses that is being supplied by the in-package spiral coil, that is embedded inside the Init pulse generator. The spiral coil is built in the LGA substrate , and the sensor consists of two chips, that are placed on opposite sides of the spiral coil, therefore using the area required for the coil and decreasing the size of the sensor chips. In this circuit Init pulses are being supplied to the TMR.

4.4.2 Low frequency noise analysis

The system noise can be divided into two different parts, one originating from the intrinsic 1/f noise which is already present in the magnetometer itself while the other one comes from the signal conditioning circuit. In the following paragraph, the main noise sources of the whole system would be detailed.

The magnetic sensor forms the first stage of the circuit, and hence constitutes a magnetoresistive Wheatstone bridge configuration. The nominal value of

the resistors is given by Rb,n = 850 Ω and the bridge output sensitivity is s_b = s_{AMR} Vb = 160 µV/ µT, where s_{AMR} = 32 µV V^{-1} µT^{-1} is the sensitivity of the AMR and the bridge voltage is given by Vb= 5 V. Therefore, the Johnson noise of the bridge resistance creates white-noise floor, at 300K and it is given as :

$$S_{AMR,T}^{1/2} = \sqrt{4k_B T R_{b,n}} = 3.75 \ nV \ Hz^{-1/2} \tag{4.15}$$

Where k_B represents the Boltzmann constant. The sensor's voltage noise is converted into magnetic field noise which is referred to the input divided by the bridge sensitivity.

$$S_{AMR,T}^{1/2} = \frac{S_{AMR,T}^{1/2}}{s_{AMR}*V_b} = 27.6 \ pT \ Hz^{-1/2} \tag{4.16}$$

On assuming additive noise, it can be deduced , the higher the sensor sensitivity or bridge voltage, the lower would be the magnetic field noise. The corner frequency of the 1/f noise at low frequencies is approximately 60 Hz, which leads to a sensor noise level of 21 nT/√Hz at 0.1 mHz. Hence, only the low frequency contribution from the AMR is sufficient enough to exceed the requirements mentioned in Eqn(2). However, apart from the intrinsic 1/f behaviour, the contributions that exists due to the thermal drifts, deteriorate the noise performance. Therefore, to overcome these limitations, the scheme mentioned in Fig. 4.17 had been implemented.

Therefore, while taking in consideration about the noise contribution of the signal conditioning circuit, the value of apportionment of the bridge drive circuit is highly negligible in comparison to the sensor noise. In order to reduce drifts, interference or noise in the analog-to-digital conversion process, ratiometric measurements are performed . Therefore, the reference voltage of the analog-to-digital converter (ADC) is also employed for driving the bridge. Later, amplification of the bridge output occurs by using space qualified low-noise instrumentation amplifiers (AD620 & AD8220) depending on the type of sensor which is being used as the magnetometer (AMR, TMR) with a gain of 603 for the AMR manufactured by Honeywell (HMC1001), 225.5 for the TMR manufactured by Crocus Technology and 10 for the TMR manufactured by MDT. AD620 is used for the signal conditioning circuit of AMR since it has low resistance and current noise is not dominant whereas the voltage noise is dominant. In case of the signal conditioning circuit of TMR, AD8220 is used, which comprises high resistance of 50 kΩ and current noise is dominant. Taking into consideration, the IA noise contribution can be modelled as :

$$\varepsilon_{o,IA}^2 = [\varepsilon_{n,IA}^2 \left(1 + \frac{f_{o,en}}{f}\right) + i_{n,IA}^2 (1 + \frac{f_{o,in}}{f}) R_b^2] \tag{4.17}$$

Where $e_{n,IA}$ = 9 nV/√Hz , $I_{n,IA}$ = 1.417e-12 A/√Hz, $f_{c,en}$ = 10 Hz and $f_{c,in}$= 200 Hz for AD620 while for AD8220, $e_{n,IA}$ = 14 nV/√Hz, $I_{n,IA}$ = 3.1639e-14 A/√Hz, $f_{c,en}$ = 20 Hz and $f_{c,in}$= 1000 Hz are the input voltage/current spectral densities and their respective corner frequencies which describes the noise characteristic of the particular IA. The input signal to the amplifier, i.e, the signal from the magnetometer, is modulated by the application of flipping pulses. However, the flipping pulses are only applicable for AMR and the instrumentation amplifier used for the signal conditioning circuit of AMR sensor is AD620, while for TMR, it is AD8220 and the field pulses that have been applied for the initialization of the circuit is known as "Init pulses" .

The phase sensitive detector is synchronized with the flipping pulses with the use of an analog switch, that alternates the sign of the unity gain amplifier for rectifying the modulated signal. The contribution of noise for both non-inverting and inverting amplifier are not critical in deducing the overall noise of the signal conditioning circuit.

The output of the signal conditioning circuit is digitised with a commercial data acquisition board (NI USB-6212). The maximum value of the rms noise of the embedded ADC is $4.524 * 10^{-6}$ V/√Hz which is given by the manufacturer. Hence, the spectral noise density is given by the formula $S_{ADC}^{1/2} = \frac{\sigma_{ADC}}{\sqrt{fs/2}}$, where σ_{ADC} represents the rms (random noise) noise in the dynamic range of +1v to -1V of the ADC and the ADC used for the experiments is 16 bits, with a full-scale range of 1V ($\pm$5V). The quantization noise of the ADC is dominated by the contribution of the spectral noise density. The manufacturer of the ADC didn't provide the low noise characteristics, thus the corner frequency of the 1/f noise has been found at 10 mHz with the help of an experimental fit to the data.

Therefore, as it has been expected before, the most significant contribution at sub-millihertz frequencies is the intrinsic 1/f noise of the AMR sensor, that has been minimized using flipping technique in the experimental results. The 1/f noise of the sensor can be reduced but it is not possible to eliminate it , as this noise will continue to be the most dominant source on the overall noise measurements of the system. Most significantly, the resistors in the bridge suffers from 1/f noise, and the AC modulation of the bridge output is unable to eliminate it. The signal conditioning circuit contributes to the electronic noise which is below the magnetic requirement along the measurement bandwidth. On utilizing the different noise reduction techniques, the noise measurement of the sensor is possible to be improved. The ADC, IA and Johnson noise of the magnetoresistances are able to limit the noise performances at frequencies much higher than 1 Hz, which is outside the LISA bandwidth.

Chapter 5

RESULTS

It can be seen from the noise measurements of the instrument amplifiers (IA) that have been tested for their use in the signal conditioning circuit, that only two IA, AD8220 and AD620 are used for TMR and AMR sensor analysis and testing.

The reason as to why this IA, AD620 was used for the signal conditioning circuit of AMR since it has low resistance and current noise is not dominant whereas the voltage noise is dominant. In case of the signal conditioning circuit of TMR, AD8220 is used, because this IA has high resistance and current noise is dominant, which is clearly evident in the following graph which shows that AD8220 has the lowest noise.
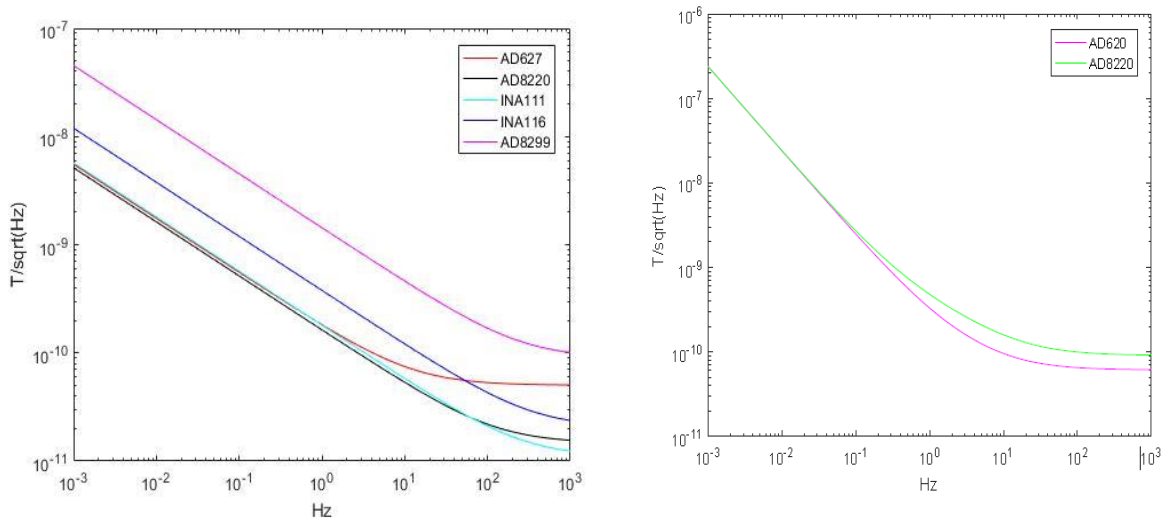
Fig 31: (a)Comparative analysis of the best fit instrumentation amplifier for the magnetic sensor. (b) Comparison of the noise density of the AD620 and AD8220 instrument amplifier

Tunnel magnetoresistance (TMR) sensors, have been analysed and experimentally tested for this project in order to investigate whether these magnetic tunnel junction sensors meet the LISA requirements in terms of detecting gravitational waves at low frequency and also to analyse the performance of noise from both intrinsic and extrinsic sources on this sensor. Hence, we tested two TMR sensors, one of them manufactured by MultiDimension technology and the other being manufactured by Crocus Technology. The TMR result that have been obtained shows that the TMR sensor manufactured by Crocus Technology is not so highly sensitive for detecting weak magnetic field but it has been used as a comparison of the noise performance and sensitivity of the TMR sensors.to suit our purpose. The lower part of the graph is dominated by the noise of data acquisition board. It is clearly evident from the power spectral density of these two sensors, only the one manufactured by MDT has been able to reach 10nT/√Hz, which is the requirement for LISA mission.

Fig. 32 : This graph shows the noise density of the circuit without the sensor
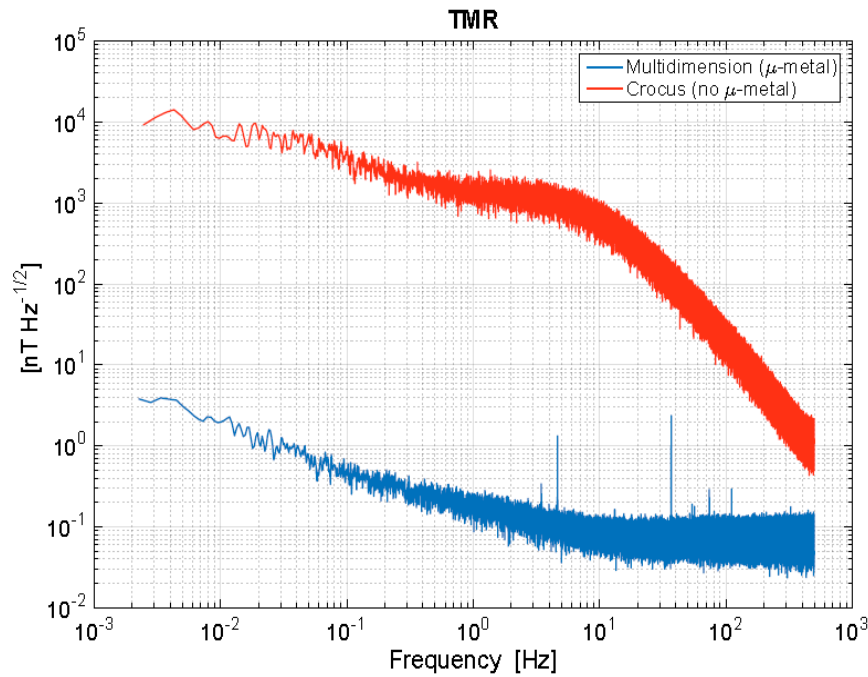
Fig 32 : Comparative analysis of the noise performance of the commercial TMR sensors
(TMR9112, CT219)

The output of TMR sensor that have been tested, are sampled in two frequencies – 1KHz and 100 Hz to see if there is extra noise at higher frequencies while the mu-metal shielding protects the magnetic sensor from the influence of external magnetic fields. Moreover, a long duration of data acquisition of the TMR sensor at 100 Hz, has helped us in reaching the benchmark of 10 nT/√Hz. The differences in noise above 10 Hz in the graphs is due to noise contribution of ADC of the data acquisition board. The internal amplifier of the board and ADC does not antialiasing filter and all noise above half the sampling frequency is aliased in the signal bandwidth. It does not change the 1/f noise because its spectral density is several orders of magnitude higher. Only the flat part in the graph which represents the white noise, is increased by a factor of √10.
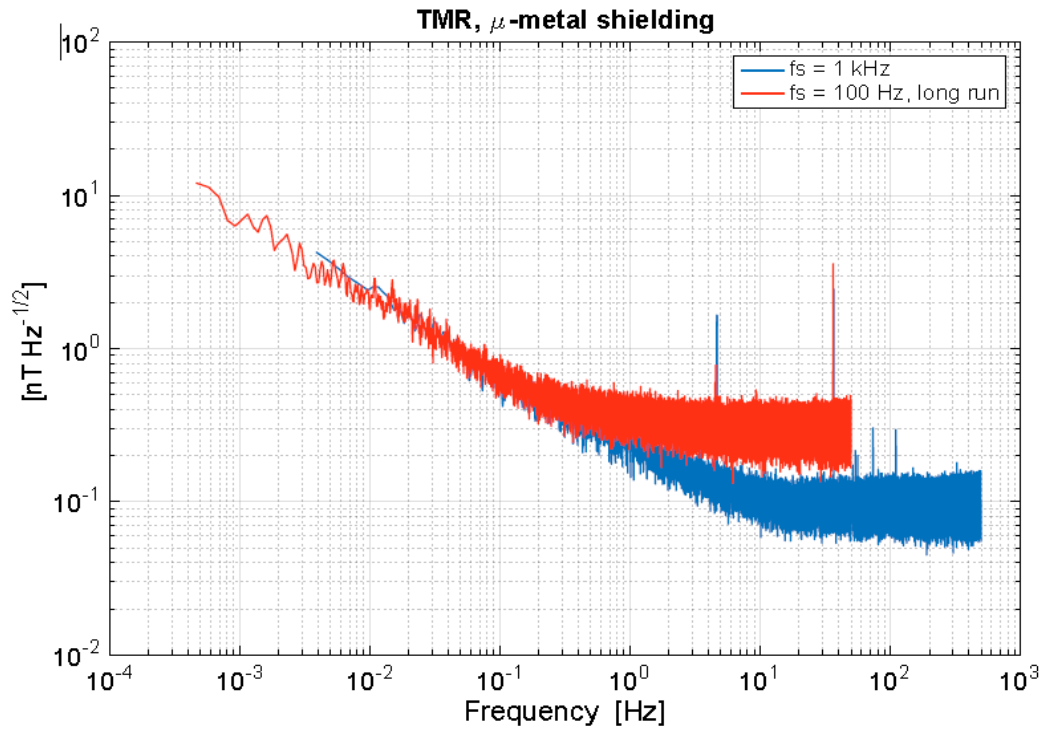
Fig 33 : The spectral noise density of the TMR9112 at two different sampling frequencies(1kHz, 100 Hz)

The TMR sensors are highly sensitive and the signal conditioning circuit in order to acquire data from the sensor needs to be tested first, otherwise a slight error or change in the circuit might affect the sensor output drastically. Therefore, AMR sensors were tested and the noise sources affecting the sensor readings were identified so as to design and develop the signal conditioning circuit of the TMR sensor , non-erroneously. The following figure provides the PSD results of the tests made with AMR sensor.
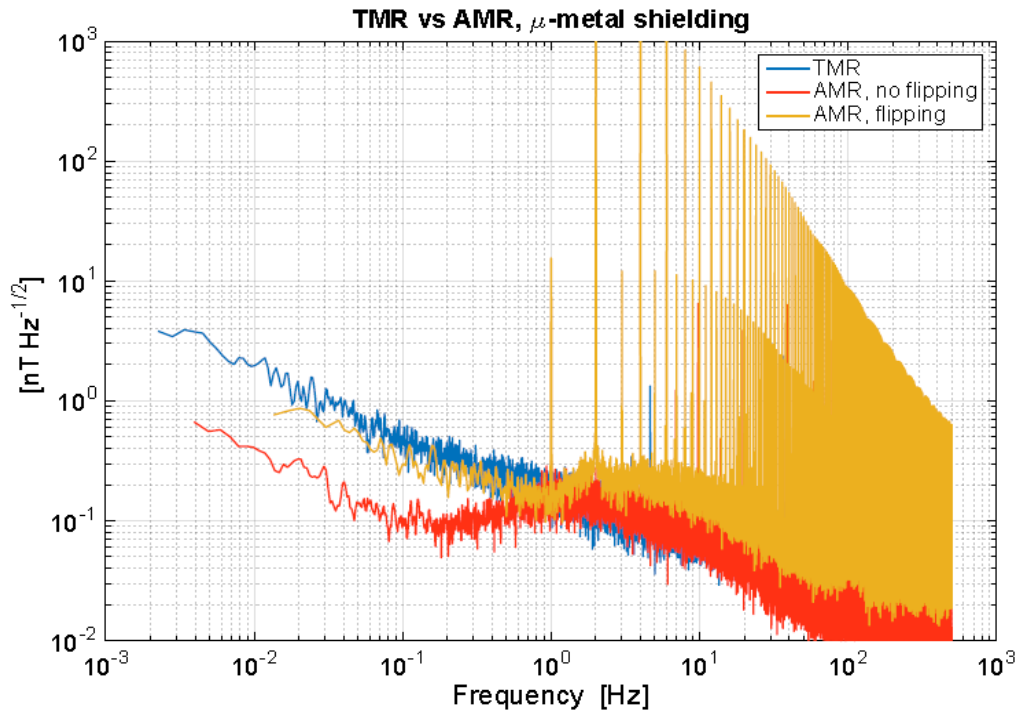
Fig.34 : This figure shows the comparative analysis of the spectral noise density of the AMR sensor HMC1001 (both with flipping and without flipping mechanism) and the TMR sensor TMR9112 with mu-metal shielding

It is quite evident from the graph that TMR has a better spectral density and more stable while taking readings for long durations inside the mu-metal shielding. The noise is much lower when the TMR9112 sensor was tested and it meets the requirements of the LISA bandwidth, thereby attaining the desired noise performance. However, in order to get much better result, longer duration runs of the sensor is needed so as to reach 1e-4 Hz.

Chapter 5

CONCLUSION

In this project, the low frequency noise characterization of an improved magnetic measuring system based on TMR has been presented with the help of a signal conditioning circuit in order to test this advanced magnetic sensor to check whether it's use as a space magnetometer is going to be viable or not for fulfilling the mission objectives of the advanced LISA mission. Magnetic Tunnel Junction (MTJ) based sensors appears as a promising solution to the problems faced while using the bulky fluxgate magnetometers or AMR sensors in the LISA Pathfinder mission. However, magnetic tunnel junction based sensors and magnetoresistors exhibits higher intrinsic noise characteristics compared to fluxgate magnetometers. Therefore, in order to improve the noise performance, different methods have been analysed and tested in the low frequency domain. In case of AMR, we have tested the flipping mechanism for reducing the 1/f noise while for the TMR sensor, the flipping circuit was integrated. The 1/f noise reduction cannot be avoided using the conventional lock-in amplification techniques (AC excitation if the bridge). The TMR sensor has been analysed and tested in this project and it has given promising results given the fact, that it has higher sensitivity level with respect to AMR. However, extra care had to be taken while handling the TMR sensor along with its signal conditioning circuit since its highly sensitive and while taking measurements with this sensor, even a certain movement of a finger can affect its output result as noise or distortions. Thus, from the achieved noise performance, TMR sensors can be considered as a potential alternative to the fluxgate sensors and AMR sensors used in LISA Pathfinder. However, space grade tests, calibrations and intrinsic noise reduction procedures needs to be conducted for the TMR sensor to be considered as the best alternative to be flown aboard the advanced LISA mission as a replacement of AMR and fluxgate magnetometer. This advanced technology can be useful for space applications, with restrictions strictly based on size, weight, power consumption and high sensitivity at low frequencies. The performance characteristics, provided by the manufacturer of this sensor can be found in the Appendix.

BIBLIOGRAPHY

[1]   M. Armano *et al.*, "Sub-Femto-   g   Free Fall for Space-Based Gravitational Wave Observatories: LISA Pathfinder Results," *Phys. Rev. Lett.*, vol. 116, no. 23, p. 231101, Jun. 2016.

[2]   M. Diaz-aguiló, I. Mateos, J. Ramos-castro, A. Lobo, and E. García-berro, "Design of the magnetic diagnostics unit onboard LISA Pathfinder," vol. 26, pp. 53–59, 2013.

[3]   I. M. Mart, "Design and assessment of a low-frequency magnetic measurement system for e LISA," 2015.

[4]   "LIGO : the Laser Interferometer Gravitational-Wave Observatory," vol. 076901.

[5]   H. Ara, "LISA and LISA PathFinder , the endeavour to detect low frequency GWs arXiv : gr-qc / 0612152v1 23 Dec 2006."

[6]   M. Armano *et al.*, "Beyond the Required LISA Free-Fall Performance: New LISA Pathfinder Results down to 20 µhz," *Phys. Rev. Lett.*, vol. 120, no. 6, p. 61101, 2018.

[7]   T. D. K. Corporation, "Characteristics of TMR Angle Sensors," pp. 1–5.

[8]   "NPTEL :: Physics - Physics of Magnetic Recording and Recording Media." .

[9]   U. Miniature, T. Fluxgate Magnetometer, and B. Aerospace&defense, "T F M 100G4," 2005.

[10]   A. Einstein, "Die Grundlage der allgemeinen Relativitätstheorie," *Ann. Phys.*, vol. 354, no. 7, pp. 769–822, 1916.

[11]   I. Mateos, J. Ramos-castro, and A. Lobo, "Sensors and Actuators A : Physical Low-frequency noise characterization of a magnetic field monitoring system using an anisotropic magnetoresistance," *Sensors Actuators A. Phys.*, vol. 235, pp. 57–63, 2015.

[12]   F. Range, "1- and 2-Axis Magnetic Sensors," pp. 1–15.

[13]   L. Tmr and I. Coil, "TMR9112."

[14]   A. Einstein and N. Rosen, "ON GRAVITATIONAL WAVES," vol. 98, no. I, pp. 43–54, 1966.

[15]   K. Riles, "Gravitational waves: Sources, detectors and searches," *Prog. Part. Nucl. Phys.*, vol. 68, no. 1, pp. 1–54, 2013.

[16]   I. M. Martín, "Design and assessment of a low-frequency magnetic measurement system for eLISA," 2015.

[17]   "Gravitational Waves and Experimental Gravity," *66th Rencontres Moriond*, no. Gravitational Waves and Experimental Gravity, 2011.

[18]   R. Weiss, "Electronically Coupled Broadband Gravitational Antenna," no. 105, 1972.

[19]   B Caron et al, "The Virgo interferometer," *Class. Quantum Gravity*, vol. 14, no. 6, p. 1461, 1997.

[20]   B. Willke *et al.*, "The GEO 600 gravitational wave detector," *Class. Quantum Gravity*, vol. 19, no. September 2001, p. 1377, 2002.

[21]   H. Search, C. Journals, A. Contact, M. Iopscience, Q. Grav, and I. P. Address, "Japanese large-scale interferometers," vol. 1237.

[22]   M. Armano and L. Pathfinder, "LISA Pathfinder : the complexity of free fall," 2017.

[23]   S. Vitale, "Space-borne gravitational wave observatories," *Gen. Relativ. Gravit.*, vol. 46, no. 5, pp. 1–19, 2014.

[24]   D. A. Shaddock, "An overview of the laser interferometer space antenna," *Publ. Astron. Soc. Aust.*, vol. 26, no. 2, pp. 128–132, 2009.

[25]   H. Araújo *et al.*, "LISA and LISA PathFinder, the endeavour to detect low frequency

GWs," 2006.

[26] M. Nofrarias Serra, J. Alberto Lobo Gutiérrez Tutor, and E. Verdaguer Oms, "Thermal Diagnostics in the LISA Technology Package Experiment," 2007.

[27] M. Díaz-Aguiló, E. García-Berro, a Lobo, N. Mateos, F. Gibert, and J. Sanjuán, "Magnetic Diagnostics Algorithms for LISA Pathfinder," \Jpcs, vol. 228, p. 12038, 2011.

[28] S. Vitale, "Science Requirements and Top-level Architecture De_finition for the Lisa Technology Package (LTP) on Board LISA Pathfi_nder (SMART-2).," Italy, 2005.

[29] M. V Balabas, D. Budker, J. Kitching, P. D. D. Schwindt, and J. E. Stalnaker, "Magnetometry with millimeter-scale antirelaxation-coated alkali-metal vapor cells."

[30] by Marc ıaz-Aguií and E. Gar ıa–Berro Montilla Alberto Lobo Gutí errez, "Magnetic Diagnostics Algorithms for LISA Pathfinder: System Identification and Data Analysis," 2011.

[31] A. Prof, J. Ramos, and M. Nofrarias, "Comparative Analysis of Different Magnetometers for eLISA mission," no. i, pp. 1–5, 2015.

[32] J. Ramos, "DDS THERMAL DIAGNOSTIC PROTOTYPE DDS-LTP," 2005.

[33] A. Fert, "Nobel Lecture: Origin, development, and future of spintronics *," *Rev. Mod. Phys.*, vol. 80.

[34] C. Duret and S. Ueno, "TMR : A New Frontier for Magnetic Sensing," no. 80, pp. 64–71, 2012.

[35] M. Julliere, "TUNNELING BETWEEN FERROMAGNETIC FILMS," 1975.

[36] J. S. Moodera, L. R. Kinder, T. M. Wong, and R. Meservey, "Large Magnetoresistance at Room Temperature in Ferromagnetic Thin Film Tunnel Junctions," *Phys. Rev. Lett.*, vol. 74, no. 16, pp. 3273–3276, Apr. 1995.

[37] Z. Q. Lei *et al.*, "Review of Noise Sources in Magnetic Tunnel Junction Sensors," vol. 47, no. 3, pp. 602–612, 2011.

[38] R. Guerrero, F. G. Aliev, Y. Tserkovnyak, T. S. Santos, and J. S. Moodera, "Shot noise in magnetic tunnel junctions: Evidence for sequential tunneling," *Phys. Rev. Lett.*, vol. 97, no. 26, pp. 1–4, 2006.

[39] L. Jiang *et al.*, "Low-frequency magnetic and resistance noise in magnetic tunnel junctions," *Phys. Rev. B - Condens. Matter Mater. Phys.*, vol. 69, no. 5, pp. 1–9, 2004.

[40] L. Jiang *et al.*, "Low-frequency magnetic and resistance noise in magnetic tunnel junctions."

[41] H. T. Hardner, M. B. Weissman, M. B. Salamon, and S. S. P. Parkin, "Fluctuation-dissipation relation for giant magnetoresistive 1/ ƒ noise," *Phys. Rev. B*, vol. 48, no. 21, pp. 16156–16159, Dec. 1993.

[42] S. Ingvarsson, G. Xiao, S. S. P. Parkin, W. J. Gallagher, G. Grinstein, and R. H. Koch, "Low-Frequency Magnetic Noise in Micron-Scale Magnetic Tunnel Junctions," 2000.

[43] N. Smith and P. Arnett, "White-noise magnetization fluctuations in magnetoresistive heads," *Appl. Phys. Lett.*, vol. 78, no. 10, pp. 1448–1450, Mar. 2001.

[44] S. Kogan, *Electronic noise and fluctuations in solids*. Cambridge University Press, 1996.

[45] M. E. Welland and R. H. Koch, "Spatial location of electron trapping defects on silicon by scanning tunneling microscopy," *Appl. Phys. Lett.*, vol. 48, no. 11, pp. 724–726, Mar. 1986.

[46] Z. Q. Lei, G. J. Li, W. F. Egelhoff, P. T. Lai, and P. W. T. Pong, "Review of Noise Sources in Magnetic Tunnel Junction Sensors," *IEEE Trans. Magn.*, vol. 47, no. 3, 2011.

[47] A. F. Md Nor, T. Daibou, M. Oogane, Y. Ando, and T. Miyazaki, "Boron effects on noise in magnetic tunnel junctions," *J. Magn. Magn. Mater.*, vol. 310, no. 2, pp. 1917–1919,

Mar. 2007.

[48] K. Kandiah and F. B. Whiting, "LOW FREQUENCY NOISE IN JUNCTION FIELD EFFECT TRANSISTORS."

[49] J. M. Almeida and P. P. Freitas, "Field detection in MgO magnetic tunnel junctions with superparamagnetic free layer and magnetic flux concentrators Field detection in MgO magnetic tunnel junctions with superparamagnetic free layer and magnetic flux concentrators," vol. 722, no. 2009, pp. 1–4, 2012.

[50] W. S. Sp and O. S. Elektryk, "Modern magnetic field sensors – a review," no. 10, pp. 1–12, 2013.

[51] R. Further, "Proton magnetometer," pp. 2–4, 1967.

[52] Honeywell, "1- and 2-Axis Magnetic Sensors HMC1001/1002/1021/1022," *Honeywell Datasheet*, pp. 1–15, 2008.

[53] Crocus Technology, "No Title."

[54] H. Hauser, P. L. Fulmek, P. Haumer, M. Vopalensky, and P. Ripka, "Flipping field and stability in anisotropic magnetoresistive sensors," vol. 106, pp. 121–125, 2003.
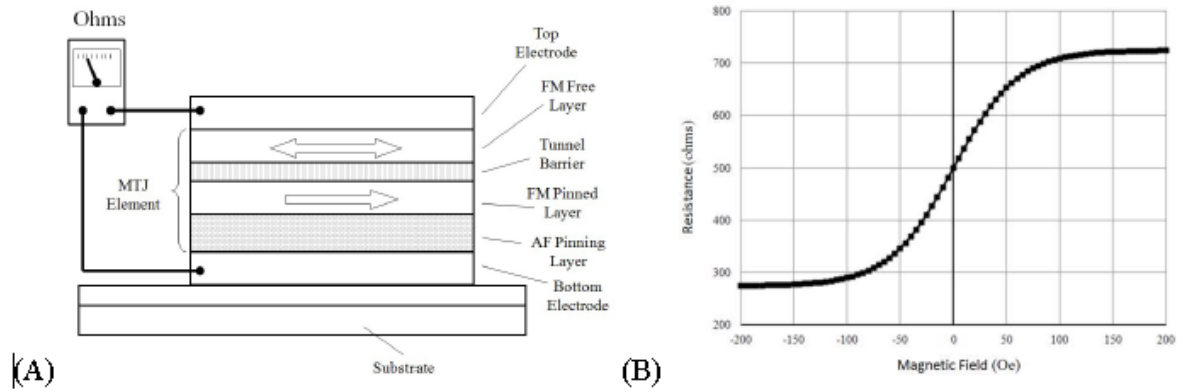
APPENDIX

Appendix 1.1 :

Fig 1 : (A) It shows the cross-section illustrating the various layers of a TMR sensor element, and (B) It shows the magnetoresistive response of a TMR sensor element

Pin Configuration

(Arrow indicates direction of applied field that generates a positive output voltage.)

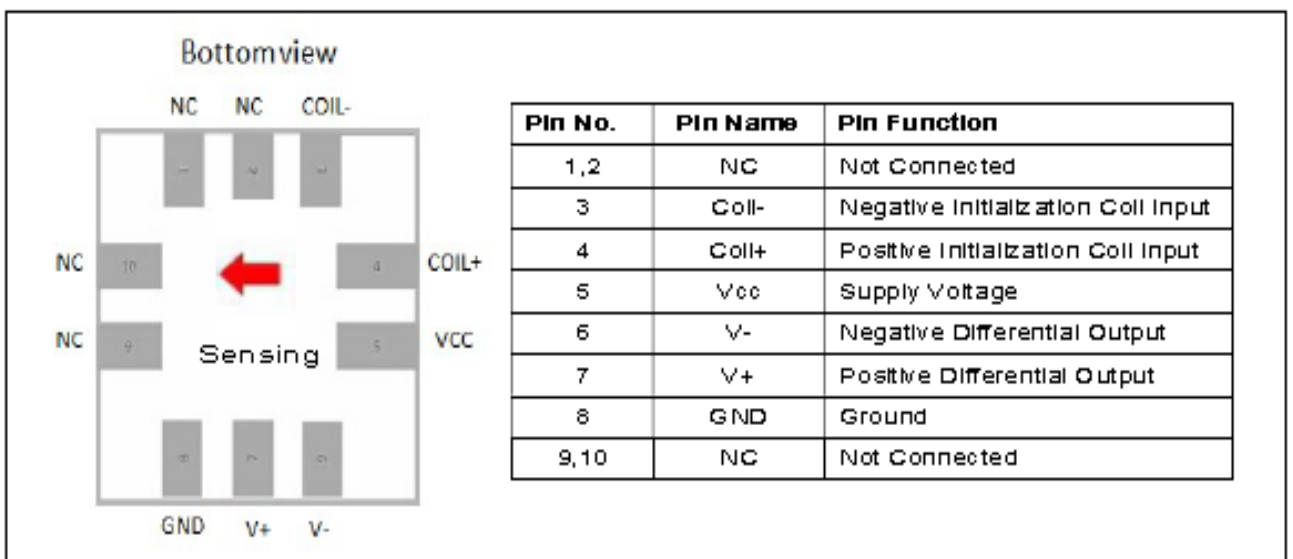| Pin No.	Pin Name	Pin Function
1,2	NC	Not Connected
3	Coil-	Negative Initialization Coil Input
4	Coil+	Positive Initialization Coil Input
5	Vcc	Supply Voltage
6	V-	Negative Differential Output
7	V+	Positive Differential Output
8	GND	Ground
9,10	NC	Not Connected

Fig. 2 : Pin out configuration of TMR9112 sensor
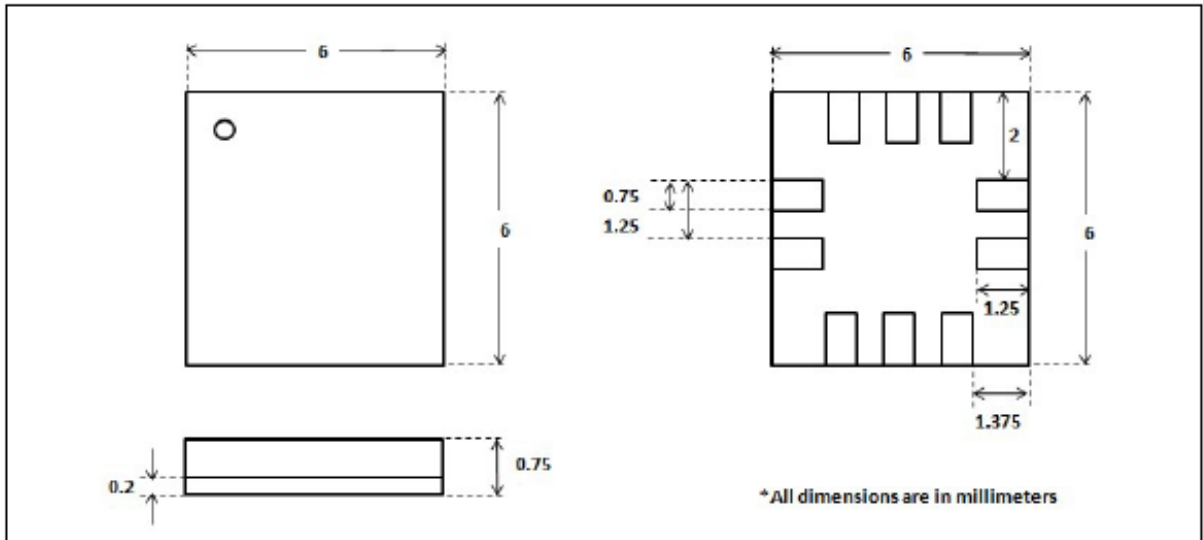
Package Information

Fig 3: Package information of TMR9112 sensor
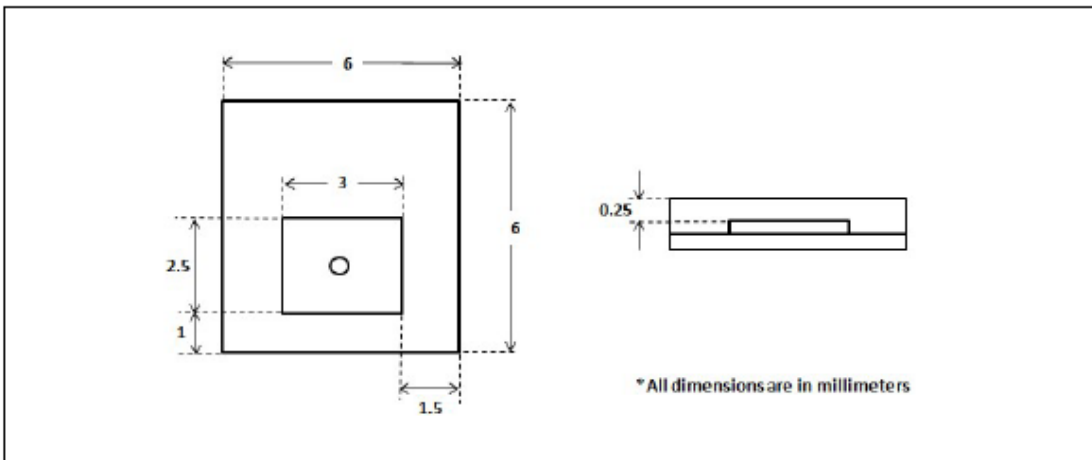
TMR Sensor Position

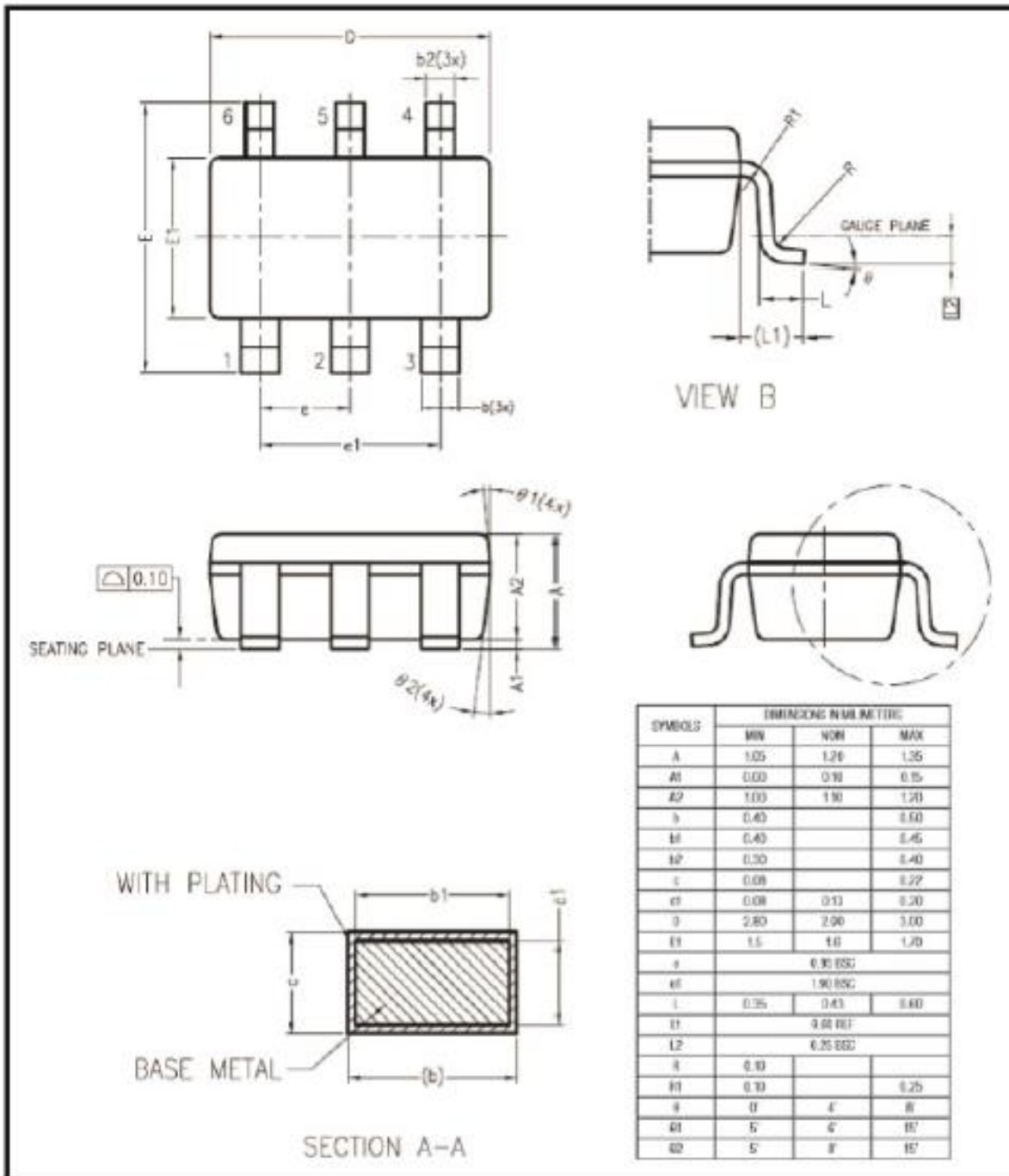Fig. 4 : TMR9112 Sensor Position

Figure 5: Package Dimensions

Fig. 5 : Package dimensions of CT219 TMR sensor by Crocus Technology

HMC1001/1002 SPECIFICATIONS

Characteristics	Conditions*	Min	Typ	Max	Units
Bridge Elements					
Supply	Vbridge (Vb) referenced to GND	-	5.0	12	Volts
Resistance	Bridge current = 10mA per bridge	600	850	1200	ohms
Operating Temperature	Ambient	-55		150	°C
Storage Temperature	Ambient, unbiased	-55		175	°C
Field Range	Full scale (FS) – total applied field	-2		+2	gauss
Linearity Error	Best fit straight line ± 1 gauss ± 2 gauss		0.1 1.0	0.5 2.0	%FS
Hysteresis Error	3 sweeps across ±2 gauss		0.05	0.10	%FS
Repeatability Error	3 sweeps across ±2 gauss		0.05	0.10	%FS
S/R Repeatability	Output variation after alternate S/R pulses Vb = 5V, I$_{SR}$ = 3A			100	µV
Bridge Offset	Offset = (OUT+) – (OUT-) Field = 0 gauss after Set pulse, Vb = 8V	-60	-15	+30	mV
Sensitivity	Set/Reset Current = 3A	2.5	3.2	4.0	mV/V/gauss
Noise Density	@ 1Hz, Vb=5V		29		nV/sqrt Hz
Resolution	10Hz Bandwidth, Vb=5V		27		µgauss
Bandwidth	Magnetic signal (lower limit = DC)		5		MHz
Disturbing Field	Sensitivity starts to degrade. Use S/R pulse to restore sensitivity.	5			gauss
Sensitivity Tempco	T$_A$= -40 to 125°C, Vb=8V T$_A$= -40 to 125°C, Ibridge=5mA	-0.32	-0.30 -0.06	-0.28	%/°C
Bridge Offset Tempco	T$_A$= -40 to 125°C, No Set/Reset T$_A$= -40 to 125°C, With Set/Reset		±0.03 ±0.001		%/°C
Bridge Ohmic Tempco	T$_A$= -40 to 125°C		0.25		%/°C
Cross-Axis Effect	Cross field = 1 gauss, Happlied = ±1 gauss With set/reset		±3 ±0.5		%FS
Max. Exposed Field	No perming effect on zero reading			10000	gauss

Fig. 6 : Technical specifications of HMC1001/1002

```
%parameters
Kv =9e-9 ; %V^2/sqrt(Hz)
Fcv = 11; %A^2/sqrt(Hz)
Ki = 6e-13; %A/sqrt(Hz)
Fci= 200; %Hz
G = 82; %gain
Ri= 50e3; %ohm  Output resistance of the sensor
%starting the loop
f =[1; 0.1; 0.01;  0.001];
f=(0.001:0.001:1000);
%calculating the noise of instrumentation amplifier
%En(s)= (Kv.^2).*(1 + Fcv./f); %V^2/Hz
En1=EnaoTMR_IA_AD620( f );
In2=In1TMR_IA_AD620( f ); %A^2/Hz
Sno1=Sensor_nosieTMR9112(f);  % Sesnor Noise
%In order to calculate the total noise of the IA, we need to calculate the
%bridge output impedance & multiplexer impedance

%calculation of bridge circuit
R = 2*(Ri.^2/(2*Ri));
%final equation for calculating noise
Enoise = sqrt(En1.^2/G.^2 + En1.^2 + (In2*Ri).^2);
%disp(Enoise)
%loglog(f,Enoise)   %Bode plot
 % We divide by the sensitivity of the sensor and Gauss to Tesla to convert to equivalent noise magnetic field
EnoiseT= sqrt((Sno1).^2 + (Enoise/(100e-3*1/1e-4)).^2);

%figure
%hold on
loglog(f,EnoiseT,'b')   %Bode plot
```

```
function [ x ] = In1TMR_IA_AD620( f )
%UNTITLED2 Summary of this function goes here
Ki = 6e-13; %A/sqrt(Hz)
Fci= 200; %Hz


x=sqrt( (Ki.^2).*(1 + Fci./f)); %A^2/Hz
end

function [ y ] = EnaoTMR_IA_AD620( f )
%UNTITLED2 Summary of this function goes here
%    Detailed explanation goes here
    Kv = 9e-9 ; %V^2/sqrt(Hz) AD620TMR
    Fcv = 11; %A^2/sqrt(Hz)


    y= sqrt((Kv.^2).*(1 + Fcv./f));
end
```

Fig. 6: Sensor Noise Calculation using IA AD620

```
%parameters
Kv = 14e-9 ; %V^2/sqrt(Hz)
Fcv = 20; %A^2/sqrt(Hz)
Ki = 1e-15; %A/sqrt(Hz)
Fci= 1000; %Hz
G = 82; %gain
Ri= 850; %ohm
%starting the loop
f =[1; 0.1; 0.01;  0.001];
f=(0.001:0.001:1000);
%calculating the noise of instrumentation amplifier
%En(s)= (Kv.^2).*(1 + Fcv./f); %V^2/Hz
En1=EnaoTMR_IA_AD8220(f);
In2=In1TMR_IA_AD8220(f); %A^2/Hz
Sno=Sensor_nosieHMC1001(f);  % Sesnor Noise
%In order to calculate the total noise of the IA, we need to calculate the
%bridge output impedance & multiplexer impedance

%calculation of bridge circuit
R = 2*(Ri.^2/2*Ri).^2;
%final equation for calculating noise
Enoise = sqrt(En1.^2/G.^2 + En1.^2 + (In2*Ri).^2+Sno.^2);
%disp(Enoise)
%loglog(f,Enoise)  %Bode plot
 % We divide by the sensitivity of the sensor and Gauss to Tesla to convert to equivalent noise magnetic field
EnoiseT=Enoise/(3.2e-3*5/1e-4);

%figure
hold on
loglog(f,EnoiseT,'g')  %Bode plot
```

Fig 7 : Sensor Noise calculation using IA AD8220

```
fs=100;
NFFT=100000;
filename='tmr_noflip_crocus5_1V.tdms';
Nmax=1e7; %Maximum number of samples to read. If the file has less it will read until the end
%crocus tech tmr sensor calculations
[x, rawdata1] = tdmsreader(filename, 1, Nmax);
%[y, rawdata2] = tdmsreader(filename, 2, Nmax);
%x2=xa(10e3:110e3);
%y2=ya(10e3:110e3);
%x2=x;1
%y2=y;
px1= pwelch(x,NFFT,50,NFFT,fs);
f=(0:length(px1)-1)/NFFT*fs;
figure
loglog (f,sqrt(px1)/225.5/75) ;
% NFFT=1024;
%px2= pwelch(y,NFFT,50,NFFT,fs);
%f=(0:length(px2)-1)/NFFT*fs;
%hold on
%loglog (f,sqrt(px2)/603,'r');
legend('x signal','y signal')
title(filename)
%title('NRSE')
%title('RSE')

figure
plot(x)
title(['Time signal ' filename])
```

Fig. 8 : PSD calculation of CT219 sensor using output from the signal conditioning circuit with the help of ADC.